Applied Catalysis B: Environmental 243 (2019) 641–656

Contents lists available at ScienceDirect

Applied Catalysis B: Environmental

journal homepage: www.elsevier.com/locate/apcatb

Highly efficient and selective electrooxidation of glucose and xylose in alkaline medium at carbon supported alloyed PdAu nanocatalysts

Thibault Rafaïdeen, Stève Baranton, Christophe Coutanceau*

IC2MP, UMR CNRS, Université de Poitiers no 7285, 4 rue Michel Brunet, TSA 51106, 86073, Poitiers cedex 9, France

ARTICLE INFO

Keywords:
Electrolysis
Glucose
Xylose
PdAu/C catalysts
Selectivity

ABSTRACT

The effect of the composition of carbon supported PdAu nanomaterials toward electrocatalytic oxidation of glucose and xylose was evaluated in alkaline medium. Pd_xAu_{10-x}/C catalysts were synthesized by a water-in-oil microemulsion method and characterized by physical (TGA, AAS, TEM, XRD) and electrochemical methods. Bulk Pd/Au alloys were formed, but the surface composition was different than the bulk one. The surface of Pd_xAu_{10-x}/C catalysts as determined by electrochemical method were enriched in Pd with respect to the nanoparticle bulk composition as determined by atomic absorption spectroscopy (AAS). Electrochemical experiments combined with in situ infrared spectroscopy measurements showed the dissociative adsorption of aldoses on Pd-rich catalysts at low potentials (appearance of the typical band of CO_{ads} on Pd surface). For catalysts with Au at. % ≥70%, this band was not visible. Pd_3Au_7/C catalyst provided the lowest oxidation onset potential, the highest activity and the best selectivity towards gluconate and xylonate. Therefore, long term chronoamperometry measurements of glucose and xylose electrooxidation were performed on this catalyst in a 25 cm^2 geometric active surface area electrolysis cell at a voltage of 0.4 V and at 293 K. Reaction products were analyzed by HPLC every hour, and by ^{1}H NMR at the end of the experiments. The main products were gluconate and xylonate. Glucose oxidation led to selectivity in gluconate of 87% for 67% conversion, and higher for lower conversion. Xylose oxidation led to selectivity in xylonate of 100% after 1 and 2 h electrolysis and of 92% after 6 h (52% conversion). The conversion of glucose and xylose into gluconate and xylonate was performed with high selectivity and an energy cost below 36 € per ton of reaction products.

1. Introduction

Xylonic and gluconic acids belong both to the top-30 list of value added chemicals from biomass [1]. They can indeed be used in numerous applications, such as building blocks for the syntheses of various biodegradable chemicals, chelating agents, additives for cement, concrete, food and pharmaceutical, *etc*. [2,3]. For these reasons, different chemical and biotechnological methods have been developed for the oxidation of glucose and xylose into gluconic (gluconate) and xylonic (xylonate) acids, respectively. Gluconic acid is produced at the industrial scale by fermentation processes that involve *Aspergillus niger* or *Gluconobacter suboxidans* bacteria [4]. The synthesis of xylonic acid from xylose using bacteria has also been reported, but to date not at the industrial scale production [2]. Although such biotechnological processes show generally acceptable selectivity, their main drawbacks concerns the low conversion rate, microbe separation, the control of byproducts, and the disposal of waste water produced by the industrial fermentation process. Therefore, the heterogeneous catalytic oxidation of carbohydrates has been proposed as a challenging but attractive process for industry [5,6].

Numerous works have been devoted to the study of glucose and xylose oxidation in aqueous media, mainly on noble metals supported on MgO, γ-Al_2O_3, carbon black *etc*., in presence of oxygen, air or hydrogen peroxide as oxidant. Generally, Pt-based catalysts led to poor selectivity with breaking of the C−C bond and formation of byproducts [6,7]. According to Onda et al. [7], a Pd/C catalyst led to lower yield in gluconic acid than a Pt/C catalyst (*ca*. 15.5% and 45%, respectively, in NaOH 1.0 mol L^{-1} aqueous solution under bubbling air after 2 h reaction at T = 353 K). On the other hand, Mirescu and Prüße reported selectivities of 99% and 96% towards xylonic and gluconic acids for the oxidation reaction of xylose and glucose, respectively, at a 4.6% Pd/Al_2O_3 catalyst in aqueous solution at pH = 9.2 under oxygen bubbling at T = 313 K. The selectivity dropped down to 80% and 83% with a 5% Pt/ Al_2O_3 catalyst [8]. Pd catalysts are indeed generally described in the literature as relatively selective for glucose oxidation [9], and their activity and selectivity can still be improved by modification with, for

* Corresponding author.
E-mail address: christophe.coutanceau@univ-poitiers.fr (C. Coutanceau).

https://doi.org/10.1016/j.apcatb.2018.11.006
Received 24 August 2018; Received in revised form 27 October 2018; Accepted 2 November 2018
Available online 05 November 2018

example, bismuth [10,11]. However, the problem of bismuth leaching [9,12] leads to decrease the durability of catalysts and makes them inappropriate for food and pharmaceutical applications. Gold catalysts have also shown very promising results in terms of activity and selectivity for the aldose oxidation reaction [13,14]. For example, Mirescu and Prüße [8] reported selectivities higher than 99.5% towards xylonic and gluconic acids for the oxidation reaction of xylose and glucose, respectively, at a 0.45% Au/TiO_2 catalyst in aqueous solution at pH = 9.2 under oxygen bubbling at T = 313 K. Other authors achieved 100% selectivity using gold colloids immobilized on carbon [13] or using gold nanoparticles supported on alumina prepared by the incipient wetness method [15]. The reader could find more information on gold-catalyzed glucose oxidation in presence of oxygen or H_2O_2 in the review of Della Pina and Falletta [16]. Generally, the aldose oxidation by heterogeneous catalysis are performed at temperatures higher than 40 °C to activate the reactions and in the presence of an oxidant as oxygen source (oxygen or hydrogen peroxide). But, Bujak et al. [17] have shown that the pre-activation by ultrasounds of silica-supported nanogold suspended in 30% hydrogen peroxide led to very active and selective catalysts for the oxidation of glucose at room temperature. More recently, the oxidation of glucose was performed in a 35% H_2O_2 aqueous solution with $FeSO_4$ as catalyst using low frequency ultrasounds as non-thermal activation process. The so-called sono-Fenton process ($FeSO_4/H_2O_2$/ultrasound) allowed achieving 95% selectivity towards gluconic acid at low temperature (297.65 K) [18]. Microwave were also used for activating selectively the conversion of glucose and derivatives [19]. A conversion of 99% and a selectivity of 96% could be obtained using an Au/Al_2O_3 catalyst at 60 °C and in the presence of hydrogen peroxide. These recent results highlight the role of non-thermal activation processes for achieving high activity and selectivity.

Electrochemical methods are also non-thermal activation processes that can be used for the controlled oxidation reactions of organic molecules. These processes have the advantages to allow the accurate control of both the activity of the reaction by modifying the catalyst structure/composition and the selectivity of the reaction by accurately tuning the anode potential (cell voltage), which control both the water and the saccharides adsorption/activation at the catalyst surface [20–24]. Indeed, in electrochemical methods, water molecules can be activated at the solid electrode materials to provide extra-oxygen atoms for the oxidation reaction of organic compounds, which allow avoiding the addition of oxidative agents in the reaction medium. The reactants are then only water as oxygen source, solid electrode materials and electrons, which contributes to make electrocatalysis a more sustainable process than catalysis. The reactions are carried out at low temperatures (293 K in the present case), *i.e.* without external power supply for the heater and without temperature control system, and in the only presence of saccharides, water and electrolyte (Na^+/OH^-).

Strangely, the great majority of papers dealing with glucose electrooxidation considers only direct glucose fuel cell [25,26], or sensor applications [26–28]. In such applications, the activity of the electrocatalysts is more important that its selectivity because high power densities and low detection limits are required, respectively. The electrooxidation of glucose at different catalytic metals has then been extensively studied, while literature concerning that of xylose is scarcer [29,30]. The most studied catalytic metals are platinum and gold, because they display good activity for these reactions. While platinum shows relatively good activity towards glucose oxidation in acidic media, gold exhibits higher oxidation rate in alkaline media [25]. Moreover, during the oxidation process, platinum tends to deactivate, due to the formation of adsorbed CO species at its surface [31]. This clearly indicates that platinum is able to break the C—C bond and therefore is non-selective for sugar electrooxidation. In the case of gold, Tominaga et al. [32] showed on the basis of surface enhanced infrared adsorption spectroscopic measurements and electrochemical quartz crystal microbalance measurements that the deactivation of the surface was only due to the formation of a close-packed vertically adsorbed gluconic or xylonic acid molecules. One method to avoid such poisoning effect is to alloy gold with a second metal. As mentioned above, Pd catalysts are relatively selective for aldose oxidation [9]. Moreover, it has been shown that interactions between gold and palladium led to enhance the activity for glucose oxidation and the selectivity towards gluconic acid. These bimetallic catalysts displayed similar performances than those achieved with the best Bi-Pd/C catalysts, without metal leaching [33]. Yan et al. [34] have studied the electrocatalytic behavior of non-alloyed PdAu/C catalysts and found a higher poisoning tolerance during glucose oxidation with a Pd_3Au_7/C composition. It has also been shown that PdAu bimetallic catalyst led to higher activity than the pure metals for glycerol electrooxidation [20,35].

Based on these bibliographic data, the objective of this contribution is to evaluate the electrocatalytic behavior at room temperature of mono-metallic Pd/C, Au/C and alloyed bi-metallic Pd_xAu_{10-x}/C catalyst (x = 1, 3, 5, 7, 9) with different atomic compositions towards glucose and xylose electro-oxidation. Because glucose is more reactive in alkaline medium than in acidic one [36], and due to the use of gold which is not electroactive in acidic media, an alkaline medium (aqueous 0.1 M NaOH electrolyte) was chosen for the study. The activity will be determined by cyclic voltammetry, whereas the reaction products and intermediates will be monitored by *in-situ* infrared spectroscopy under potential control. Particularly, this last technique will allow determining the potential region where the oxidation of monosaccharides occurs without C—C bond breaking. At last, the most promising catalyst in terms of activity and selectivity will be used in the anode of a 25 cm^2 geometric active surface area electrolysis cell for product accumulation. Analysis of the reaction products during long-term chronoamperometry experiments at a cell voltage of 0.4 V will be made by ^{1}H NMR and HPLC.

2. Experimental

2.1. Synthesis of catalysts

The Pd_xAu_{10-x}/C (x = 0, 1, 3, 5, 7, 9, 10) catalysts were prepared using a water-in-oil microemulsion method. [37–39], Briefly, appropriate amounts of potassium tetrachloropalladate and tertrachloroauric acid trihydrate (K_2PdCl_4 and $HAuCl_4{\cdot}3\ H_2O$, 99.99% purity, Alfa Aesar) were dissolved in ultra-high purity water (Milli-Q, 18.2 MΩ cm, Millipore) in order to reach a total metal concentration of 0.1 mol L^{-1}, with Pd/Au atomic ratios of 10/0, 9/1, 7/3, 5/5, 3/7, 1/9 and 0/10. A 1.6 mL aliquot of aqueous solution containing metal salts was added to a homogeneous solution of 37 g n-heptane (99% purity, Acros Organics) and 16.1 g polyethylene glycol dodecyl ether (Brij® L4, Sigma Adrich). The mixture was stirred until a translucent and stable microemulsion was obtained. Then, 100 mg of sodium borohydride were added as reducing agent. After reduction of metal salts, a given amount of carbon powder (Vulcan XC72, Cabot Corp.) was added to the colloidal solution to reach a metal loading of 40 wt. %. The mixture was then filtered and washed several times with acetone and ultrapure water. The catalytic powder was dried under air overnight in an oven at 343 K before undergoing a thermal treatment for 2 h at 473 K under air to eliminate remaining surfactant.

2.2. Characterization of catalysts

Thermo-Gravimetric Analysis (TGA) measurements were carried out to determine the exact value of metal loading using a TA Instrument model SDT Q 600. The measurements involved gradually heating the sample from 298 K to 1173 K with a heating rate of 10 K min^{-1} under an air flow of 100 mL min^{-1}. Atomic absorption spectroscopy (AAS) analyses were carried out with a Perkin Elmer AA200 Atomic absorption spectrometer. TEM analysis was performed using a JEOL JEM 2100 (UHR) microscope with a resolution of 0.19 nm. The mean size and size distribution of the Pd_xAu_{10-x}-NPs were determined from the Feret's

diameter by counting at least 300 isolated NPs using the ImageJ free software. [40] X-ray Diffraction (XRD) patterns were acquired using PANalytical Empyrean X-ray diffractometer. Measurements were performed from $2\theta = 20^{\circ}$ to $2\theta = 110^{\circ}$ in a step mode, with a step interval of 0.06° and a fixed acquisition time of 10 s at each value of 2θ.

2.3. Electrochemical measurements

The experimental setup consisted in a thermostated classical three-electrode cell fitted with a reversible hydrogen electrode (RHE), a 0.071 cm^2 geometric surface area glassy carbon disk as substrate for the working electrode and a 8 cm^2 surface area glassy carbon plate as counter electrode. The cyclic voltammetry (CV) and linear sweep voltammetry (LSV) measurements were performed using a Voltalab PGZ402 potentiostat (Radiometer analytical) in a N_2-purged 0.1 mol L^{-1} NaOH (semiconductor grade 99.99%, Sigma-Aldrich) electrolyte at 293 K. The electrocatalytic activity of materials was evaluated at 293 K in the presence of 0.1 ml L^{-1} of glucose or xylose (99%, Sigma-Aldrich) in the electrolyte. The working electrodes were prepared by dispensing onto the glassy carbon disk 3 µL of a catalytic ink prepared as follows: first, 17.7 mg of Pd_xAu_{10-x}/C catalytic powder were added to 2.646 mL of ultra-high purity water and the suspension was homogenized using an ultrasonic bath for *ca.* 15 min; then, 354 µL of commercial solution of Nafion (only used as a binder in electrodes to avoid loss of catalytic materials) dissolved in aliphatic alcohols (5 wt. %, Sigma Aldrich) were added to the above-described suspension; the 3.00 mL Nafion-containing suspension was then homogenized in an ultrasonic bath (ultrasonic bath Fisherbrand 15051, 2.75 L, 37 kH, 320 W) for *ca.* 30 s. Considering the targeted 40 wt. % of metals in the catalytic powder for the catalyst synthesis, this procedure of electrode preparation leads to a metal loading on the electrode of 100 $\mu g_{metal}\, cm^{-2}$.

2.4. In-situ Fourier transform infrared spectroscopy (FTIRS) measurements

In situ FTIRS experiments were performed with a Bruker IFS 66 FTIR spectrometer modified for beam reflection on the electrode surface at a 65° incident angle. To remove interferences from atmospheric water and CO_2 the beam path was evacuated. An Infrared Associates liquid nitrogen-cooled HgCdTe detector was used. The spectral resolution was 4 cm^{-1}, and each spectrum was obtained by averaging 512 spectra recorded for 35 s. Spectra were recorded every 0.05 V during the linear voltammetry carried out in a 0.1 mol L^{-1} NaOH and 0.1 mol L^{-1} glucose (xylose) electrolyte at 1 mV s^{-1} (*i.e.*, each spectrum represents the average signal recorded for 0.035 V range every 0.05 V) from 0.05 to 1.15 V vs RHE. The experimental details of the electrochemical setup for SPAIRS (single potential alteration IR spectroscopy) are described elsewhere [41,42]. Spectra were normalized as follows:

$$\frac{\Delta R}{R} = \frac{R_E - R_{E_{Ref}}}{R_{E_{Ref}}} \quad (1)$$

where R_E is the reflectivity recorded at the electrode potential E during the positive potential scan and R_{ERef} is the reflectivity recorded at 0.05 V vs RHE. Therefore, negative absorption bands correspond to the formation of species at the electrode surface and positive absorption bands correspond to the consumption of species at the electrode surface.

2.5. Chronoamperometry (CA) measurements

Electrolysis measurements were conducted at 293 K in a 25 cm^2 single filter press type electrolysis cell fitted with a Pd_3Au_7/C anode (0.5 $mg_{metal}\, cm^{-2}$) and a Pt/C cathode (0.5 $mg_{Pt}\ cm^{-2}$), both separated by a simple blotting paper and mechanically pressed in the cell. Both compartments of the cell were fed in recirculation at 25 mL min^{-1} with 30 ml solution containing 0.1 mol L^{-1} NaOH and 0.1 mol L^{-1} glucose or 0.1 mol L^{-1} xylose, using a Masterflex L/S peristatic pump fitted with Norpren tubes (Masterflex precision tubing L/S 14), and rotated at 50 rpm. The current was recorded for 6 h at a cell voltage of 0.4 V. The $I_{cell}(t)$ curves were recorded by using a Voltalab PGZ402 potentiostat (Radiometer analytical) to record the applied cell voltage and the current. Fig. 1 displays the schematic representation of the filter press type electrolysis cell designed for the chronoamperometry measurements.

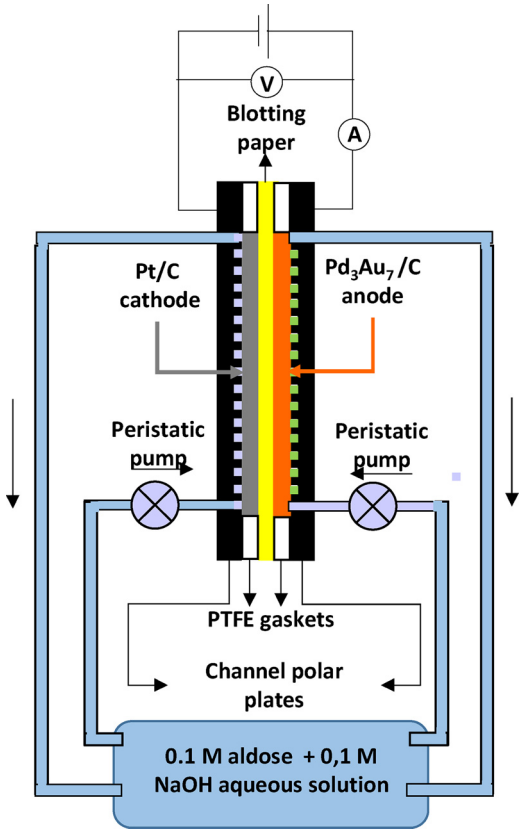

Fig. 1. Schematic representation of the electrolysis cell designed for the chronoamperometry measurements.

A 0.6 mL aliquot was taken every hour and analyzed by HPLC (Varian Prostar HPLC equipped with a Transgenomc ICSep ICE-COREGEL 107H column for organic acids, aldehydes, alcohols and ketone molecules separation). All standards corresponding to the compounds expected were prepared from sodium gluconate, lithium xylonate, tartronic acid, 2-ketogluconic acid, 5-ketogluconic acid, glucuronic acid, oxalic acid, formic acid, tartric acid, glycolic acid, L-threonic acid hemicalcium salt and glyoxylic acid from Sigma–Aldrich (purity ≥97% except for lithium xylonate, purity ≥95%). The compounds were dissolved in ultrahigh purity water with concentrations from 0.02 M to 0.1 M (with increments of 0.02 M) and neutralized with NaOH when necessary. The chromatography was performed with 0.007 mol L^{-1} H_2SO_4 aqueous solution as eluent at 0.6 mL min^{-1} flow rate with a UV detector set at $\lambda = 210$ nm. At the end of the electrolysis experiments, the solutions were analyzed by ^1H NMR (Bruker Ultrashield 400 plus with a Bruker AD-XT pump and a Bruker B-ACS 60 automatic sample changer). The samples were neutralized by HCl, lyophilized and put in D_2O (Deuterium oxide, 99.9 atom % D, Sigma Aldrich) for analysis. The remaining glucose and xylose concentrations after 6-h electrolysis were analyzed by UV–vis spectrometry (Thermo scientific Helios Omega UV–vis) after reaction with a Fehling solution (SI 1).

Table 1
Characterization data of the Pd_xAu_{10-x}/C catalysts.

		Pd	Pd_9Au_1	Pd_7Au_3	Pd_5Au_5	Pd_3Au_7			Pd_1Au_9			Au
Metal loading[a] [wt %]		40	38.7	36.2	42.7	41.3			36.9			35.4
Composition[b] [at%]	**Pd**	**100**	**90**	**80**	**58**	**23**			**13**			**0**
	Au	**0**	**10**	**20**	**42**	**77**			**87**			**100**
A[c] [Å]		3.897	3.915	3.936	3.986	4.033			4.050			4.071
L_v [nm]		2.9	3.9	3.3	3.7	5.9			6.3			4.4
Mean particle size[d] [nm]		4.0	4.5	4.3	4.4	5.8			6.4			6.8
E_{pic}[e] [V vs RHE]		0.647	0.650	0.695	0.740	0.735	0.835	1.110	0.765	0.885	1.110	1.110
Surface [%]		100	100	100	100	8	36	56	12	24	64	100
Surface alloy	**Pd**	**100**	**99**	**89**	**80**	**81**	**60**	**0 100**	**74**	**55**	**0**	**0**
composition[f] [at%]	**Au**	**0**	**1**	**11**	**20**	**19**	**40**		**26**	**45**	**100**	**100**
Global surface composition[f] [at%]	**Pd**	**100**	**99**	**89**	**80**	**28**			**22**			**0**
	Au	**0**	**1**	**11**	**20**	**72**			**78**			**100**
Charge involved in oxide reduction[f] [C]		1837	1895	930	610	46	188	219	21	41	85	272
S_{real} [cm^2]		4.33	4.48	2.35	1.54	0.12	0.51	0.78	0.06	0.11	0.31	0.97
EASA [$m^2\ g_{metal}^{-1}$]		61	63	33	22		20			7		14

[a] From TGA.
[b] From AAS.
[c] From XRD.
[d] From TEM.
[e] From cyclic voltammetry.
[f] From integration of the oxide reduction peaks.

3. Results and discussion

3.1. Physicochemical characterization of Pd_xAu_{10-x}/C materials

Table 1 gives the characterization data for the Pd_xAu_{10-x}/C materials. The actual metallic charges of the carbon-supported mono- and bi-metallic materials, as determined by TGA, are close each to the others and in accordance with the expected 40 wt % metal loading (between 34.5 and 42.7 wt %). The actual composition of the bi-metallic materials as determined by AAS are very close to the expected ones. The combination of both results confirms that metal atoms (Pd and Au) were completely incorporated in NPs during the synthesis process. To complete these data with information concerning the microstructure of the materials, XRD patterns were recorded (Fig. 2a). They were analyzed using the Levenberg-Marquardt method and deconvoluted using a pseudo-Voigt fitting by means of a computer refinement program (Fityk free software [43]). All materials exhibit diffraction peaks of the different crystallographic planes located at the characteristic positions for a face centered cubic (fcc) structure, typical of metallic Pd and Au. In the case of the Pd/C mono-metallic material, additional peaks appear (indicated with ☆ in Fig. 2a), the positions of which are typical of a tetragonal PdO phase (JCPDS 41-1107). The diffraction peaks related to this latter phase are no longer observable as soon as gold is added to palladium, even in a small content, which indicates the existence of strong interactions between both metals. Another small diffraction peak located at *ca.* 25° is attributed to the (002) plane of turbostratic graphite. The positions of diffraction peaks related to the crystallographic planes of the fcc structure are shifted towards lower 2θ value when the gold content in crystallites increases. The lattice parameters (a) determined for all materials are given in Table 1; they correspond to the average of the values obtained from the (111), (200), (220), and (311) planes, calculated using the Bragg equation [44]:

$$\frac{4\sin^2\theta}{\lambda^2} = \frac{1}{d^2} = \frac{h^2 + k^2 + l^2}{a^2} \quad (2)$$

$$\Rightarrow a = \frac{\lambda\sqrt{h^2 + k^2 + l^2}}{2\sin\theta} \quad (3)$$

where λ is the $K_{\alpha 1}$ radiation wavelength (1.5406 Å) of the Cu source, θ the angle at the maximum diffraction intensity and h, k, l the Miller indexes of crystallographic planes.

The lattice parameters calculated for the mono-metallic Pd/C and Au/C materials are consistent with those of bulk materials. The value of the lattice parameter increases linearly with the Au atomic ratio, as shown in Fig. 2b, which is also consistent with the formation of PdAu alloy structures. Additionally, XRD results confirm the compositions of materials as determined by AAS. The apparent mean crystallite sizes (L_v) have been calculated from the diffraction peak located close to $2\theta = 40°$, which corresponds to the (111) crystallographic plane of metallic palladium and gold:

$$L_v = \varphi\frac{\lambda}{\mathrm{FWHM}\cos\theta} \quad (4)$$

where φ is the shape factor ($\varphi = 0.89$ for spherical crystallite) and FWHM is the full width at half-maximum [44].

For palladium-rich materials ($5 \le x \le 10$), the crystallite size values remain almost constant, between 3 and 4 nm. But for gold-rich materials ($x < 5$), a dramatic increase of the particle size from 4 to 6 nm occurs.

Typical TEM images of some Pd_xAu_{10-x}/C materials are given in Fig. 3a,c,e,g, along with the particle size distributions in Fig. 3b,d,f,h. From these histograms, the mean particle sizes could be determined. The smaller mean size (4.0 nm) and the bigger one (6.8 nm) were obtained for the mono-metallic Pd/C and Au/C materials, respectively. The mean particle sizes of the bi-metallic nanomaterials increase with the increase of the Au atomic content in the particles, as well as the spread of the particle size distributions. The presence of big objects with sizes greater than 20 nm could be noted for materials with high Au contents (Au at. % ≥70%, Fig. 3e,g). These objects were not taken into account in the statistics for the determination of the mean particle size. TEM results are consistent with those obtained from XRD, showing that the crystallite size increased with the increase of Au content in the materials.

3.2. Electrochemical characterization of Pd_xAu_{10-x}/C materials

Fig. 4 displays the cyclic voltammograms (CV) recorded for the Pd_xAu_{10-x}/C materials at 5.0 mV s^{-1} and 293 K in a N_2-purged NaOH 0.1 M aqueous electrolyte. In the case of mono-metallic materials, the electro-active surface areas (EASA) were calculated from the integration of the current involved in the surface oxide reduction peaks centered at 0.647 V vs RHE for Pd and 1.100 V vs RHE for Au. Grdén et al. [45] showed that the potential upper limit of 1.450 V during the positive scan of the CV led to the formation of a monolayer of PdO and that

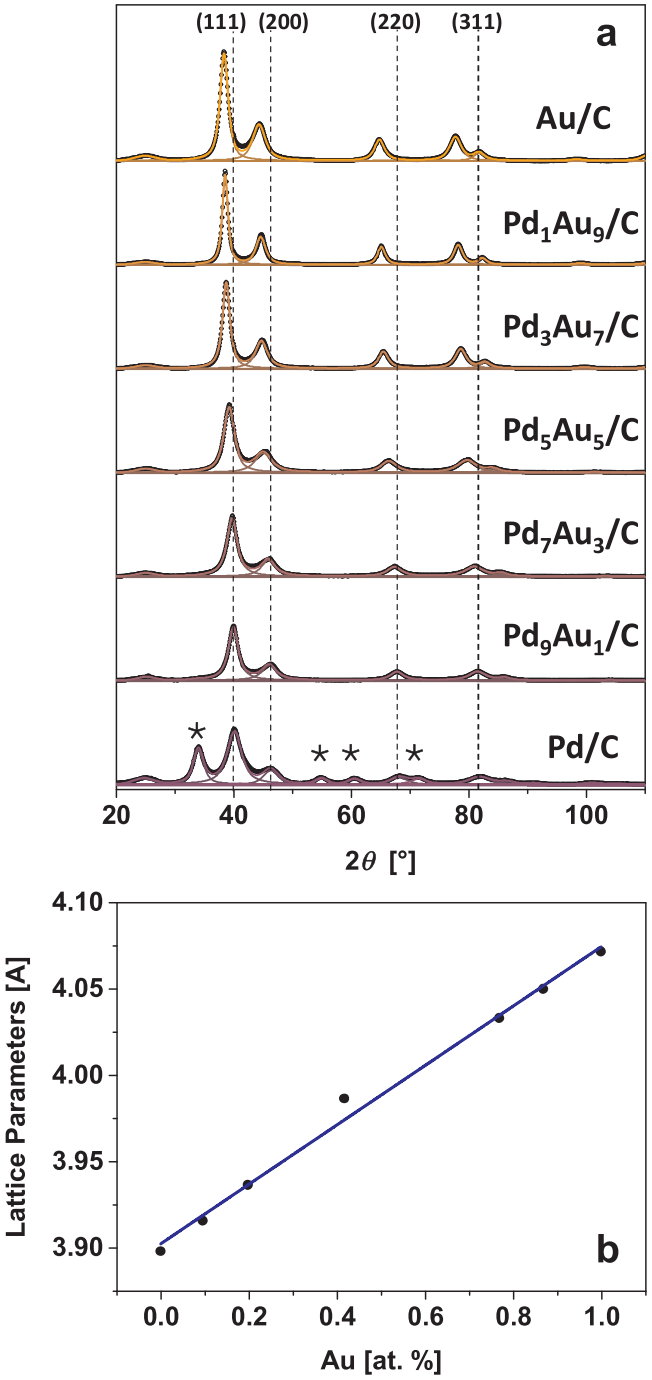

Fig. 2. (a) XRD patterns of the Pd_xAu_{10-x}/C (x = 0, 1, 3, 5, 7, 9, 10) catalysts (☆ indicates the diffraction peak relates to the tetragonal PdO structure), and (b) Graph of the related lattice parameters as a function of the Au content in catalysts.

a charge density of $Q_{Red_{theo}}^{PdO}$= 424 μC cm^{-2} was associated to the reduction of the formed PdO monolayer during the negative scan. An EASA of *ca.* 61 $m^2\,g^{-1}$ was calculated for Pd/C. The same procedure was applied for Au/C catalyst. Kahyaoglu [46] showed that the charge involved in the Au surface oxide peak reduction in NaOH 0.1 M electrolyte for the upper limit potential of the positive scan of the CV fixed at 1.450 V corresponds to $Q_{Red_{theo}}^{AuO}$= 280 μC cm^{-2}. An EASA of *ca.* 14 $m^2\,g^{-1}$ was calculated for Au/C.

Considering the CVs recorded with the bi-metallic Pd_xAu_{10-x}/C catalysts, three observations can be made: first the reduction peak at lower potential changes in position, shifting towards higher potential values when the Au content is increased; second the charge under this peak decreases when the Au content increases; third, for high Au contents (x ≥ 7), the peak at *ca.* 1.1 V vs RHE related to reduction of Au surface oxides appears and grows with the content of Au. Because electrochemical reactions take place only at the surface of the materials, these observations will help us to determine the surface composition of the catalysts, which is of primary importance for electrocatalytic reactions. To determine the surface composition, the well-established electrochemical method developed by Rand and Wood [47] was used. Such a method provides more interesting information than XPS measurement because (i) only the surface atoms which can be electro-active are probed (the mean escape depth of electrons by XPS is close to 1 nm or more for Pd and Au [48–50]), (ii) the surface compositions are determined in the environment of their use and (iii) it gives access to the surface alloy(s) composition while XPS would just give a global surface composition in Pd and Au. Rand and Wood demonstrated that the potential position of the oxide reduction peak on a PdAu surface alloy depended on its composition according to the following equations:

$$E_p^{alloy} = X_{Pd}E_P^{Pd} + X_{Au}E_p^{Au} \quad (5)$$

$$\Rightarrow X_{pd} = \frac{E_p^{alloy} - E_p^{Au}}{E_P^{Pd} - E_P^{Au}} \quad (6)$$

where X_{Pd} and X_{Au} are the Pd and Au surface atomic fractions and $E_p{}^{Pd}$ and $E_p{}^{Au}$ are the oxide reduction peak potentials for the monometallic Pd and Au nanoparticles, respectively. Results are given in Table 1. For Pd_xAu_{10-x}/C materials with low Au atomic content (x ≥ 5), a single oxide reduction peak is observed, and the surface alloy is palladium enriched when compared with the bulk ratio (Pd surface at. % > Pd bulk at. % for all catalysts). For materials with high gold contents (x ≤ 3), three reduction peaks appear, corresponding to two PdAu surface alloys with different compositions and to pure gold. The surface of materials becomes gold rich. These samples clearly present a heterogeneous distribution of palladium on the nanoparticle surface and islands of non-alloyed Au sites. Since XRD measurements, which consider the bulk of nanomaterials, indicated a linear variation of the lattice parameter with the Au atomic ratio, it can be concluded that the segregation of Pd or Au atoms, depending on the atomic ratio range, affects only the few first atomic layers of nanoparticles.

From the surface composition, the real surface area of materials (and the electroactive surface area) could be determined using the following equations [51]:

$$S_{Pd} = \frac{Q_{Red}^{PdO}}{Q_{Red_{theo}}^{PdO}} \quad (7)$$

$$S_{Au} = \frac{Q_{Red}^{AuO}}{Q_{Red_{theo}}^{AuO}} \quad (8)$$

$$S_{PdAu} = \frac{Q_{Red}^{PdAu(O)}}{Q_{Red_{theo}}^{PdO} X_{Pd} + Q_{Red_{theo}}^{AuO} X_{Au}} \quad (9)$$

where Q_{Red}^{AuO}, Q_{Red}^{PdO} and $Q_{Red}^{PdAu(O)}$ are the charges in the reduction peaks of Pd, Au and PdAu alloys, respectively; X_{Pd} and X_{Au} represent the atomic surface compositions of the Pd/Au surface alloys as determined from the Rand and Wood method.

Results are given in Table 1. The trend is that both the real surface and the electroactive surface area decrease with the increase of Au content. These results are fully consistent with previously published ones on Pd_xAu_{10-x}/C prepared by a water-in-oil microemulsion method [37,39].

3.3. Electrocatalytic activity of Pd_xAu_{10-x}/C materials

Fig. 5 displays the third (stable) polarization curves recorded at 293 K and 5 mV s^{-1} on mono-metallic Pd/C and Au/C catalysts for the

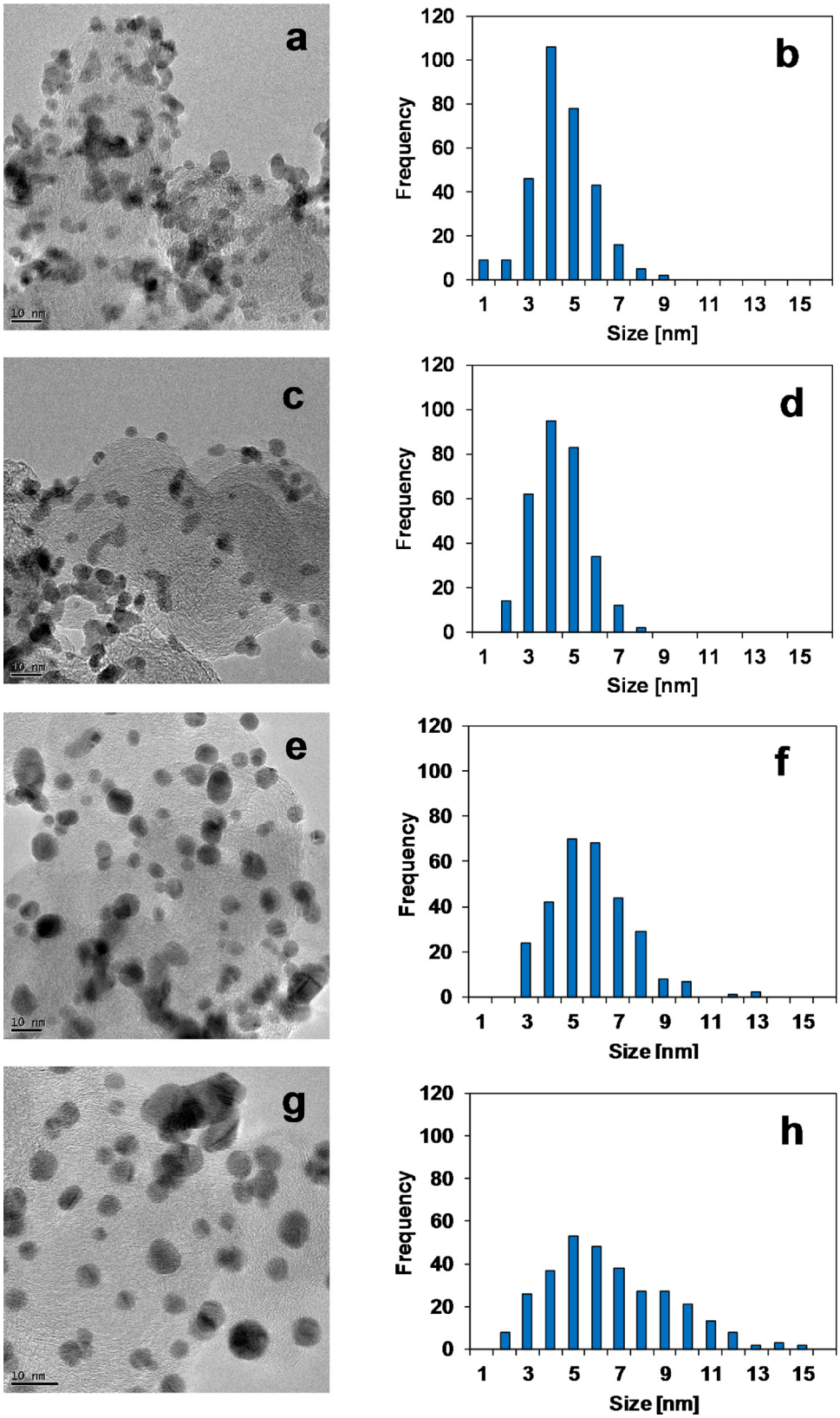

Fig. 3. TEM images and histograms of particle size distribution from TEM observations on (a,b) Pd/C, (c,d) Pd_7Au_3/C, (e,f) Pd_3Au_7/C and (g,h) Au/C.

oxidation of 0.1 mol L^{-1} glucose and 0.1 mol L^{-1} xylose in a 0.1 mol L^{-1} NaOH aqueous electrolyte. The potential scan rate of 5 mV s^{-1} is slow enough to be close to the steady state; then only the stationary faradaic currents (due to electrochemical reaction of the saccharide oxidation) are observed and the transient currents (electrosorption of species on catalyst surface and capacitive currents due to the electrode polarization) are limited to the minimum. Since the electrodes have the same geometric surface area and are loaded with the same mass of

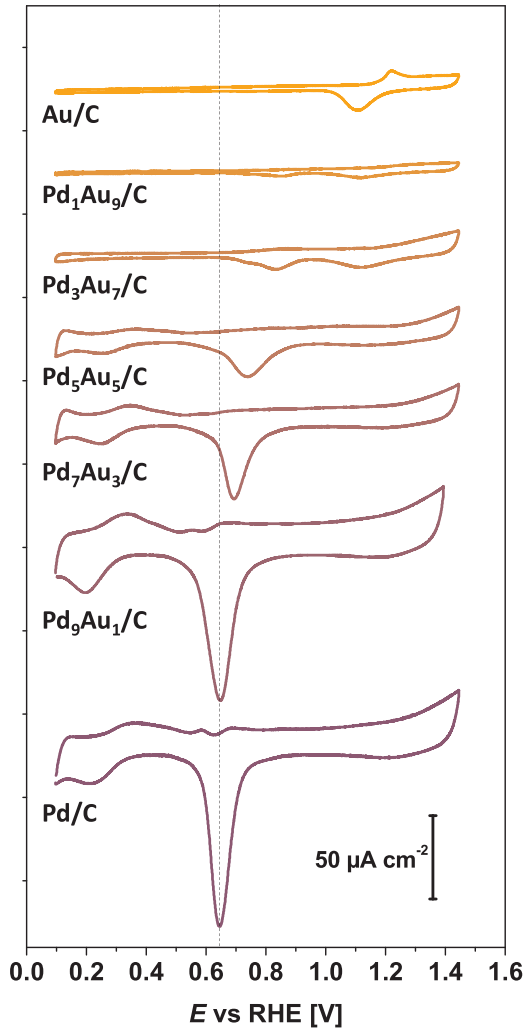

Fig. 4. Cyclic voltammograms of Pd_xAu_{1-x}/C catalysts (scan rate = 5 mV s^{-1}, N_2-purged 0.1 M NaOH electrolyte, T = 293 K, E_{max} = 1.45 V vs RHE).

catalytic powder, the polarization curves in Fig. 5a,c compare the mass activity of the catalysts towards the oxidation of monosaccharides after correction by the metal loading determined from TGA (Table 1). The Au/C catalyst displays higher mass activity than the Pd/C one at low potentials, as higher current densities are recorded on the potential range from *ca.* 0.20 V to *ca.* 0.60 V vs RHE and *ca.* 0.25 V to *ca.* 0.68 V vs RHE, for glucose and xylose oxidation reactions, respectively. For higher potentials up to 1.05 V vs RHE, Pd/C provides higher current densities than Au/C, finally, for potentials higher than 1.05 V vs RHE, the formation of an oxide surface on Pd leads to a drastic drop of activity. The specific activity, *i.e.* the catalytic activity per square centimeter of electrocatalytic metal, is dramatically higher for Au/C catalyst than for Pd/C one over the whole studied potential range (Fig. 5b,d). The second remark is that glucose is more electroreactive than xylose on both materials. For example, Fig. 5a,c clearly show that higher current densities are recorded at 0.40 V vs RHE for the glucose oxidation than for the xylose oxidation (2.58 mA cm^{-2} on Au/C and 0.92 mA cm^{-2} on Pd/C for glucose, and 1.16 mA cm^{-2} on Au/C and 0.14 mA cm^{-2} on Pd/C for xylose).

Simões et al. [20], showed that the electro-oxidation of glycerol in alkaline media started for both catalytic materials Pd/C and Au/C at the same onset potential of *ca.* 0.55 V. This was explained in terms of a Langmuir-Hinshelwood mechanism for Pd/C, *i.e.* adsorption of glycerol on the Pd surface at low potentials, activation of water molecules to form Pd-OH surface species from *ca.* 0.55 V vs RHE and reaction between adsorbed glycerol species and adsorbed OH to form the final reaction products. In the case of Au/C catalysts, the first step of glycerol electro-oxidation was the adsorption of hydroxyl ions with partial charge transfer (rate-determining step) followed by the interaction between the hydrogen atom born by the second carbon atom in the glycerol molecule and the Au-OH_{ads} species [52]. It has been proposed that the first step of glucose oxidation on Pt sites occurred *via* the adsorption of the anomeric carbon [31,53] leading further to the formation of glucono-lactone in the hydrogen potential region, which is converted into gluconate in presence of hydroxyl ions [54], and directly to carboxylate species for potentials higher than 0.6 V. Because Pt and Pd behave similarly in a catalytic point of view, the same mechanism could be proposed for the Pd/C catalyst. In the case of Au, Beden et al. [55] have shown that gold was able to adsorb OH species in alkaline media from *ca.* 0.4 V vs RHE. However, the electrooxidation reactions start at lower potentials, *i.e. ca.* 0.2 V and *ca.* 0.25 V vs. RHE for glucose and xylose, respectively (Fig. 5a,c). Therefore, the mechanism proposed for glycerol electro-oxidation doesn't apply in the case of saccharides. Adzic et al. [56] proposed that the first peak of glucose oxidation (between 0.00 and 0.60 V) could involve metallic gold surfaces, without a strong adsorption of OH^-, whereas the second one at higher potentials could coincide with the formation of an $AuOH^{(1-\lambda)-}$ layer, leading to the formation of gluconate. More recently, on the basis of the analysis of the glucose oxidation peak at potential lower than 0.6 V during the cathodic scan of a cyclic voltammogram, Pasta et al. [26] also proposed a mechanism involving the adsorption of glucose on metallic Au surface at low electrode potentials with formation of gluconolactone. It seems then that for both metals, the first intermediates formed at low potentials for glucose and xylose oxidations are lactone structures, which could remain either adsorbed on the surface or released in the reaction medium where it would be further hydrolyzed into gluconate and xylonate. In this case, the lactone structures must be more strongly adsorbed on Pd surface than on Au surface to explain the delay in oxidation onset potential between both catalysts (Fig. 5a,c). Moreover, considering the same mechanisms for glucose and xylose adsorption/oxidation, the adsorbed species from xylose seems to be more strongly adsorbed than the adsorbed species from glucose.

Fig. 6 presents the third (stable) polarization curves recorded at 5 mV s^{-1} on bi-metallic Pd_xAu_{10-x}/C catalysts for the oxidation of 0.1 mol L^{-1} glucose and 0.1 mol L^{-1} xylose in a 0.1 mol L^{-1} NaOH aqueous electrolyte. The linear scan voltammograms were recorded under the same conditions as those for monometallic Pd/C and Au/C catalysts, and the current densities were corrected from the metal loading determined by TGA (Table 1). The polarization curves of Fig. 6 compare then the mass activity of catalyst as a function of the electrode potential. For both sugars, the same trend arises. Pd-rich catalysts (bulk Au content ≤50 at. %) behave very closely to pure Pd/C one, whereas Au-rich catalysts (bulk Au content ≥70 at. %) behave almost as the pure Au/C one. These important changes in catalytic behavior are more likely related to the surface composition than to the bulk composition. Indeed, for Au bulk composition ≤50 at.% of Au, the surface of catalysts are very rich in Pd atoms (higher than 80 at. % of Pd), whereas for Au bulk composition ≥70 at. %, the surface of the catalysts becomes richer in gold (higher than 70 at. % of Au). The mass activity of catalysts at low potentials, *i.e.* the current density at a given potential between the oxidation onset potential and *ca.* 0.90 V vs RHE, increases with the increase of gold content up to 70 at. % for both sugars and then decreases towards that of pure gold. It is worth to note that, for potentials lower than 0.45 V vs RHE, both the Pd_3Au_7/C and Pd_1Au_9/C materials lead to higher catalytic activity than Au/C (Pd_3Au_7/C being the best catalyst in terms of mass activity). Fig. 7 presents as examples the CVs recorded on Pd/C and Pd_3Au_7/C for glucose and xylose electrooxidation (Fig. 7a and b, respectively). The reverse negative scan reveals that the Pd_3Au_7/C is less poisoned by adsorbed species from glucose and xylose as higher oxidation current are observed below 0.7 V vs. RHE. It is also worth to note that higher poisoning tolerance during

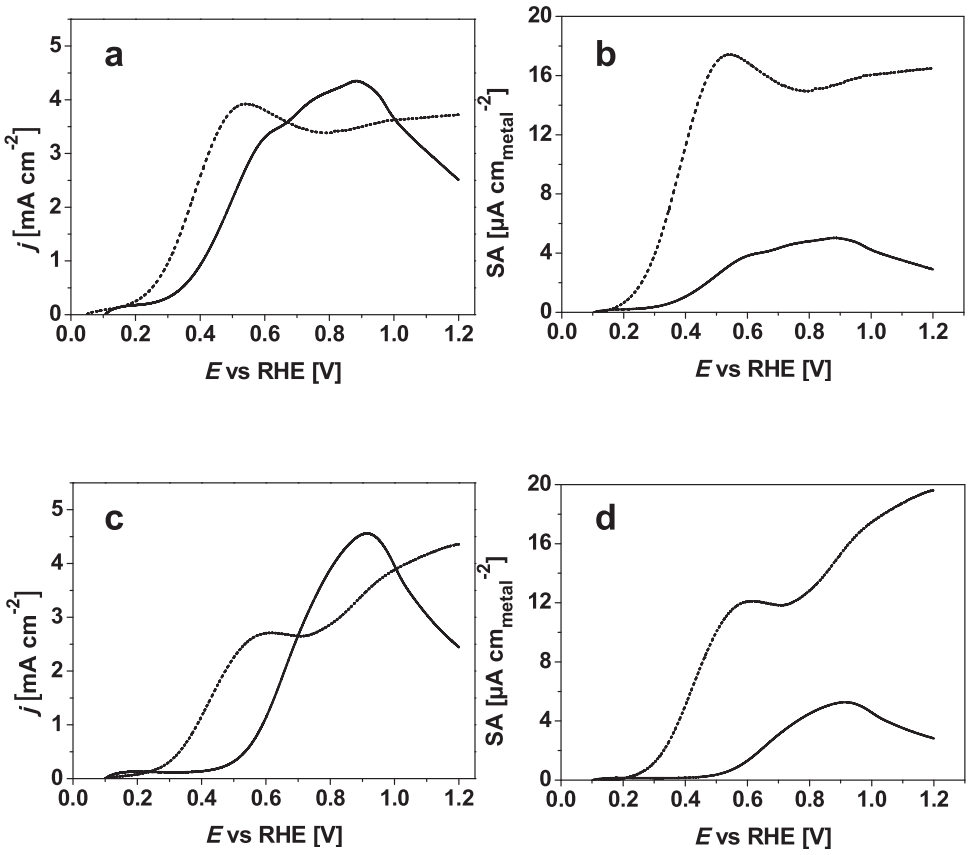

Fig. 5. Polarization curves (a) and surface activity curves (b) of 0.1 M glucose oxidation and polarization curves (c) and surface activity curves (d) of 0.1 M xylose oxidation recorded on Pd/C (solid line) and on Au/C (dotted line). Scan rate = 5 mV s^{-1}, N_2-purged 0.1 M NaOH electrolyte, T = 293 K).

glucose oxidation was obtained with our alloyed Pd_3Au_7/C catalyst than with the non-alloyed Pd_3Au_7/C catalyst by Yan et al. [34], as much lower onset potentials (*i.e.* much more active catalysts) for aldose oxidation are obtained in the present work. This suggests that obviously a synergetic effect occurs between both metals, and that the higher the interaction between Au and Pd (alloyed structures), the higher the activity is at low potentials (tolerance to poisoning). Generally, the increase of activity and/or tolerance to poisoning of bi-metallic catalysts is explained either in terms of bi-functional mechanism [57,58], or ligand effect [59,60]. The bifunctional mechanism stipulates that one of the both types of surface atoms adsorbs the organic reactant and the other adsorbs (activates) OH species from water or hydroxyl ions, providing the extra oxygen atom necessary to complete the oxidation reaction and to desorb the organic products. However, in the low potential range of catalytic activity improvement (E < 0.40 V vs RHE), none of both metals, Pd and Au, is expected to be able to adsorb (activate) OH species. The Ligand effect stipulates that the change in cell parameter by alloying Pd and Au (as demonstrated by XRD measurements) results in change in the electronic density of states close to the Fermi level, which further could modify the adsorption process and adsorption strength of species, modifying the route, intermediates and products of the electro-oxidation reaction. This last effect seems to be responsible of the catalytic improvement of Au-containing materials.

3.4. In-situ infrared spectroscopy measurements

In order to shed light on the processes taking place at the electrode/electrolyte interface, infrared spectra were recorded as a function of the electrode potential in a N_2-purged 0.1 mol L^{-1} electrolyte at 293 K and 1 mV s^{-1} for the electrooxidation of 0.1 mol L^{-1} glucose and xylose on the different catalysts (Figs. 8 and 9).

Looking first at the spectra recorded for the glucose oxidation on Pd_xAu_{10-x}/C catalysts (Fig. 8), one can remark that the infrared absorption bands in the so-called infrared fingerprint region of organic molecules, between 1000 cm^{-1} and 1600 cm^{-1}, appear at lower potentials with the increase of the Au content from 0 at. % (pure Pd/C) to 70 at. % (Pd_3Au_7/C), in agreement with the gain in activity at low potentials observed by cyclic voltammetry. The second remark is that the positions of absorption peaks on the spectra in this wavenumber region don't change with both the potential and the catalyst composition, only their intensities are varying, which indicates that same functional groups are formed or consumed at different rates.

A first group of negative absorption bands located at *ca.* 1044, 1092 and 1136 cm^{-1} (bands A, B, C in Fig. 8a) corresponds to the ν(C—O) stretching of CH_2-OH functions [31,61,62]. At higher wavenumber values, two bands appear simultaneously, a medium one at 1414 cm^{-1} and a strong one at 1581 cm^{-1} (bands D and E in Fig. 8a). The absorption bands at *ca.* 1581 cm^{-1} is associated with a shoulder at *ca.* 1680 cm^{-1} (band F in Fig. 8a and band K in Fig. 8f). In the case of the Pd_7Au_3/C catalyst a new band appears at 1734 cm^{-1} for potentials higher than 0.75 V (Band J in Fig. 8e). Between 1870 and 1920 cm^{-1}, an absorption band (band G in Fig. 8a) appears for Pd-rich Pd_xAu_{10-x}/C catalysts ($x \geq 5$) at potentials as low as 0.10 V vs RHE (Fig. 8a,b,c,d). This absorption band is typical of CO adsorbed species (CO_{ads}) on Pd surface [63], which results from the dissociative chemisorption of the glucose molecule at low potentials. The intensity of this infrared band decreases with the increase of Au content in catalytic materials, which indicates that the surface is less and less poisoned (blocked) by adsorbed CO species. For the Pd_3Au_7/C catalyst, this absorption band is no more visible (Fig. 8e), as well as for pure Au/C material (Fig. 8f), indicating that these catalysts don't have the ability to break the C—C bond at low electrode potentials. The decrease of the blocking of the Pd surface with the increase of the Au content may partly explain the improvement of the activity at low potentials. At high electrode

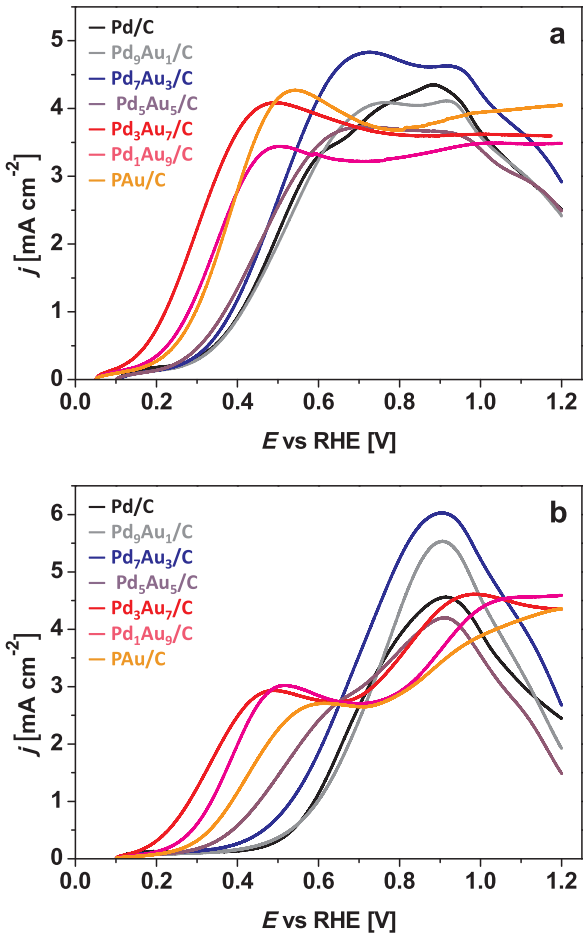

Fig. 6. Polarization curves of (a) 0.1 M glucose oxidation and of (b) 0.1 M xylose oxidation recorded on Pd/C (black line), Pd_9Au_1/C (grey line), Pd_7Au_3/C (blue line), Pd_5Au_5/C (purple line), Pd_3Au_7/C (red line), Pd_1Au_9/C (pink line) and Au/C (orange line). Scan rate = 5 mV s^{-1}, N_2-purged 0.1 M NaOH electrolyte, T = 293 K) (For interpretation of the references to colour in this figure legend, the reader is referred to the web version of this article).

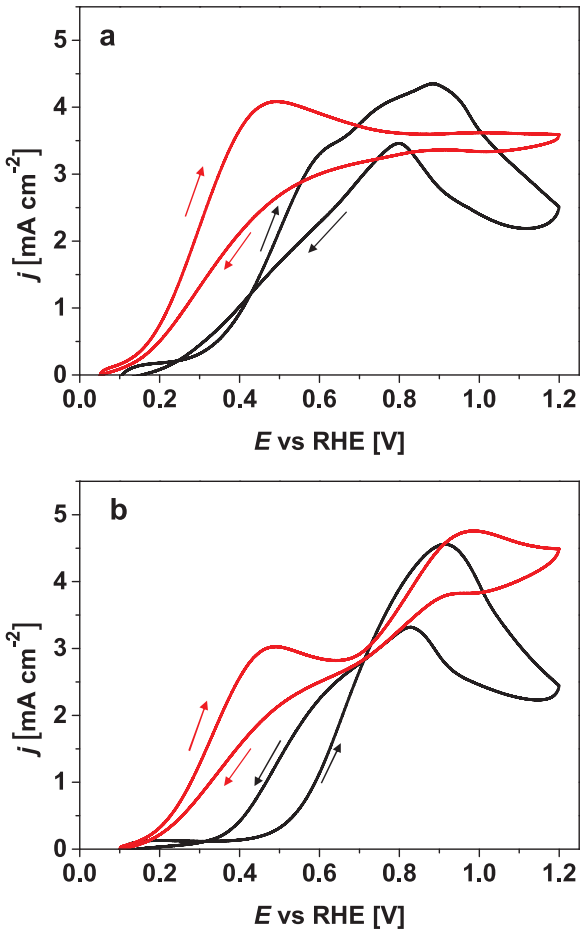

Fig. 7. Cyclic voltammograms of (a) 0.1 M glucose oxidation and of (b) 0.1 M xylose oxidation recorded on Pd/C (black line) and Pd_3Au_7/C (red line). Scan rate = 5 mV s^{-1}, N_2-purged 0.1 M NaOH electrolyte, T = 293 K) (For interpretation of the references to colour in this figure legend, the reader is referred to the web version of this article).

potentials (E > 0.70 V vs RHE), an intense peak appears at 2343 cm^{-1} (band H in Fig. 8a). This peak corresponds to the formation of interfacial CO_2 [64,65].

The band located at 1581 cm^{-1} clearly indicates the formation of carboxylate species [31,66,67], over the whole potential range where catalysts are active. The band at 1414 cm^{-1} is more difficult to assign. On the one hand, Christensen et al. [66] observed an absorption band at *ca.* 1410 cm^{-1} for the oxidation of ethylene glycol in alkaline medium and proposed that it could be due to the formation of carbonate (CO_3^{2-}). On the other hand, Beden et al. [31] proposed that both bands they observed on a Pt electrode at 1410 and 1590 cm^{-1} corresponded to gluconate. But, in the case of Pd_3Au_7/C catalyst no infrared band corresponding to adsorbed CO species is observed (no C—C bond breaking) and the absorption band at 1414 cm^{-1} appears concomitantly with the band at 1581 cm^{-1} as soon as the catalyst is active for the glucose oxidation. For this catalyst at least, this latter absorption band seems rather due to the formation of gluconate as proposed by Beden et al. [31] than to the formation of carbonates as proposed by Christensen et al. [66]. In the case of Pd-rich Pd_xAu_{10-x}/C catalysts ($x \geq 5$), the formation of a layer of adsorbed CO species at the surface of the materials as soon as 0.1 V vs RHE indicates clearly that the C—C bond could be broken, leading to a mixture of reaction products and possibly, to a contribution of carbonate formation to the absorption band at 1414cm^{-1}. In the case of Pd_xAu_{10-x}/C catalysts with $x \leq 0.3$ the C—C bond breaking is avoided, and gluconate seems to be the only product formed. The presence of gold at the surface of the catalytic nanoparticles avoids the dissociative adsorption of glucose, the formation of adsorbed CO species and further improves the activity of the catalysts at low electrode potentials. At high potentials (E > 0.7 V vs RHE), all catalysts lead to the formation of CO_2, which indicates that the C—C bond breaking occurs and that the selectivity towards gluconate decreases. However, the similarity of the spectra in the 1000–1600 cm^{-1} wavenumber range seems to indicate that gluconate is the main reaction product on all catalysts. The shoulder at 1683 cm^{-1}, as well as the peak at *ca.* 1734 cm^{-1} observed with Pd_3Au_7/C, which are both in the infrared carbonyl region, could reasonably be attributed to the formation of lactone structures [31,61,62]. But, lactones once released in the electrolyte are likely hydrolyzed in the presence of hydroxyl groups to form gluconate [31,54].

About the same remarks as above for glucose can be done from the infrared spectra recorded for the electrooxidation of xylose on the different Pd_xAu_{10-x}/C catalysts (Fig. 9). The absorption bands in the 1000–1800 cm^{-1} being located at the same wavenumber values as for glucose oxidation, it can be proposed that species with the same functionalities are formed. The CO_{ads} absorption band is again visible on Pd-rich catalysts, but no more visible with the Pd_3Au_7/C catalyst, (Fig. 9e), as well as for pure Au/C material (Fig. 9f), confirming that these catalysts don't have the ability to break C—C bonds at low electrode potentials. It is then likely that these catalysts display very high selectivity towards xylonate formation. Comparing the CO_{ads} absorption band relative intensities on Pd_xAu_{10-x}/C catalysts with $x \geq 5$ (Pd-rich catalysts)

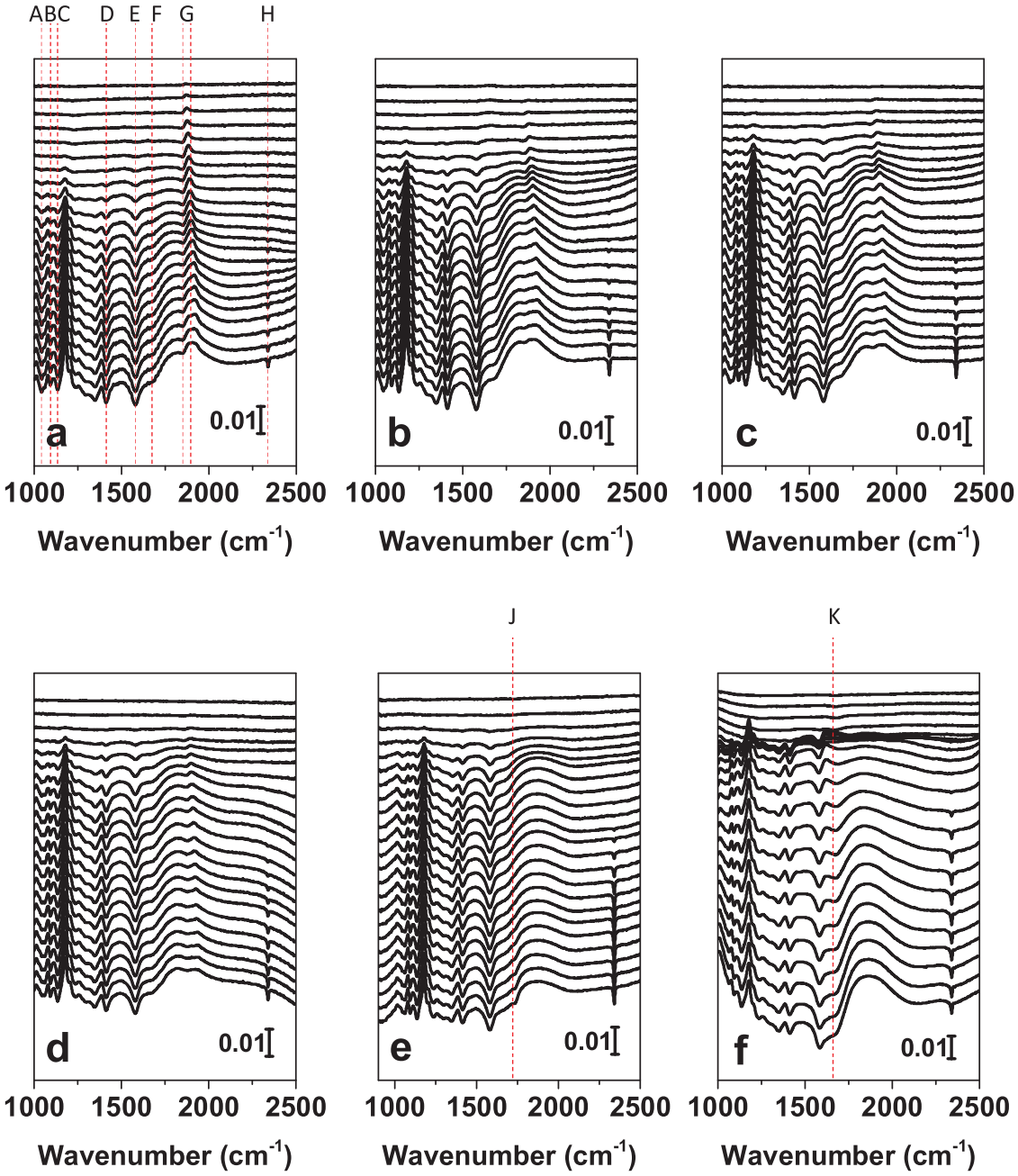

Fig. 8. Infrared spectra recorded during 0.1 M glucose oxidation in 0.1 M NaOH electrolyte on (a) Pd/C, (b) Pd_9Au_1/C, (c) Pd_7Au_3/C, (d) Pd_5Au_5/C, (e) Pd_3Au_7/C and (f) Au/C catalysts. Scan rate: 1 mV s^{-1}, resolution 4 cm^{-1}, T = 293 K. Vertical scale: $\Delta R/R$.

for the glucose and xylose oxidations, it seems that xylose is more prone to adsorb dissociatively on Pd surface than glucose; the resulting more important blocking of the surface could explain the lower reactivity of xylose as observed by voltammetry study.

From both these studies, the Pd_3Au_7/C catalyst appears to be very promising in terms of activity and of selectivity towards gluconate/xylonate formation at low electrode potentials. For these reasons, this material was chosen to perform larger scale electrolysis measurements and reaction product analysis from glucose and xylose electrooxidation.

3.5. Chronoamperometry (CA) measurements

With the objective of determining the products formed at the electrode, CA measurements were carried out in a 25 cm^2 geometric active surface area filter press type electrolysis cell at 293 K for 6 h at a constant cell voltage of 0.4 V selected from the *in situ* infrared spectroscopy results. In the cathodic compartment, the Pt/C catalyst served for the hydrogen evolution reaction (HER) according to the following reaction:

$$2H_2O + 2\,e^- \rightarrow H_2 + 2\,OH^- \quad (10)$$

The anodic reactions, assuming the formation of gluconate or xylonate are given in Eqs. (11) and (12), respectively:

$$\text{Glucose: } C_6H_{12}O_6 + 3\,OH^- \rightarrow C_6H_{11}O_7^- + 2\,H_2O + 2\,e^- \quad (11)$$

$$\text{Xylose: } C_5H_{10}O_5 + 3\,OH^- \rightarrow C_5H_9O_6^- + 2\,H_2O + 2\,e^- \quad (12)$$

The reversible potential of the H_2O/H_2 redox couple being 0.0 V vs. RHE and considering that the HER occurs with very high kinetics (low overpotentials), it can be assumed that under actual operational conditions the anode potential remains between 0.35 V and 0.4 V vs RHE.

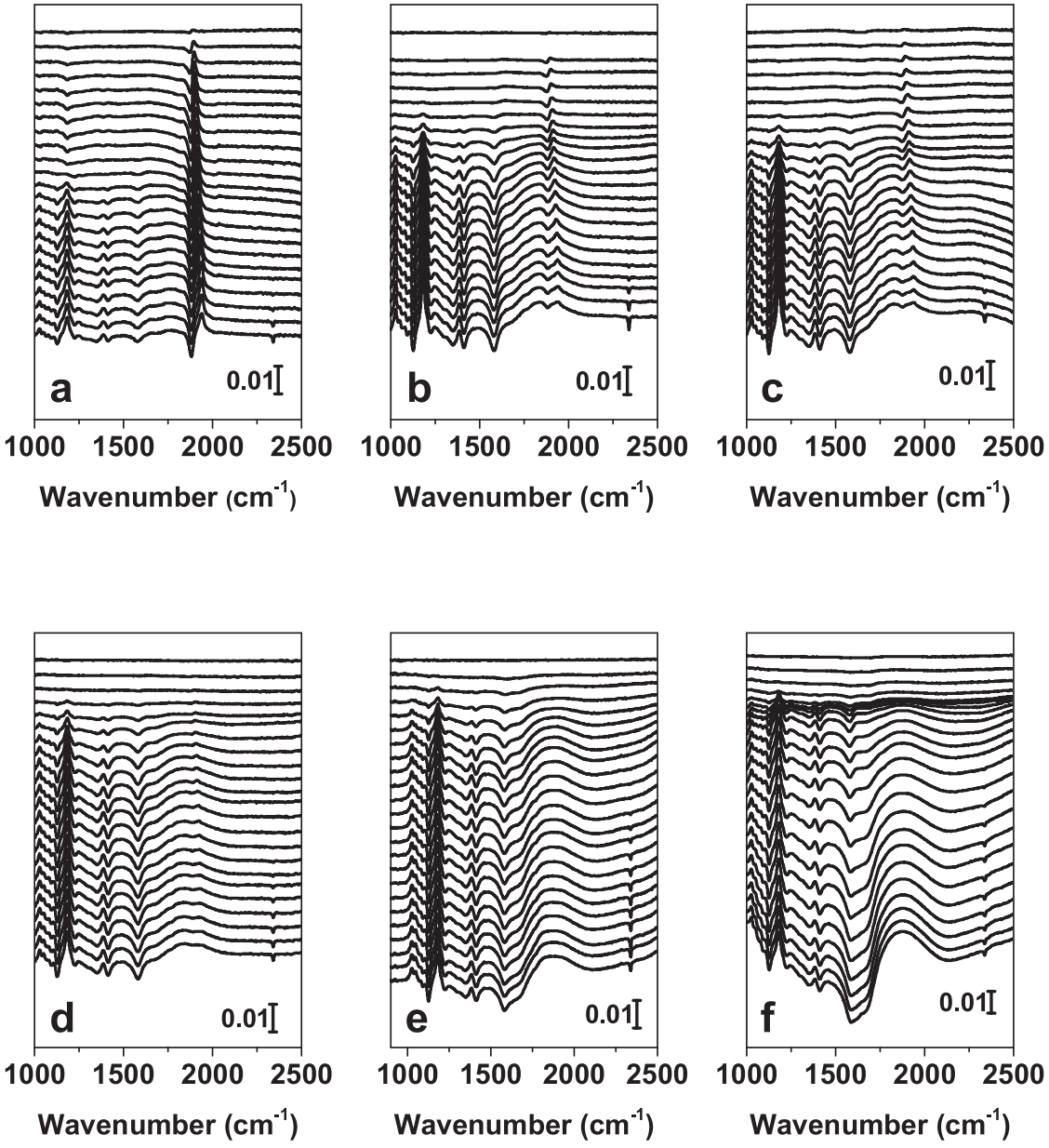

Fig. 9. Infrared spectra recorded during 0.1 M xylose oxidation in 0.1 M NaOH electrolyte on (a) Pd/C, (b) Pd_9Au_1/C, (c) Pd_7Au_3/C, (d) Pd_5Au_5/C, (e) Pd_3Au_7/C and (f) Au/C catalysts. Scan rate: 1 mV s^{-1}, resolution 4 cm^{-1}, T = 293 K. Vertical scale: $\Delta R/R$.

The shift in the anode potential was controlled during the electrolysis measurements using reversible hydrogen electrode (RHE) as reference, and it was observed that indeed it remained between 0.35 V and 0.40 V *versus* the reversible hydrogen electrode (SI 2). This result is not surprising because the cell voltage (difference between the anode potential and the cathode potential) was imposed at a value of 0.4 V. The choice of the cell voltage for electrolysis measurements was done because according to the *in situ* infrared spectroscopy measurements, the oxidation of the anomeric group of glucose or xylose into gluconate or xylonate appeared by far the main reaction pathway at so low anode potentials (very high selectivity).

In addition, because some hydroxyl ions are produced at the cathode for the hydrogen evolution reaction and consumed at the anode for the aldose electrooxidation, the pH of the solution was measured prior to and after 6 h electrolysis measurements. It was found that the pH decreased from 13 to 12.5 over the time scale of the electrolysis measurements.

Fig. 10 shows the current *versus* time curves recorded at a cell

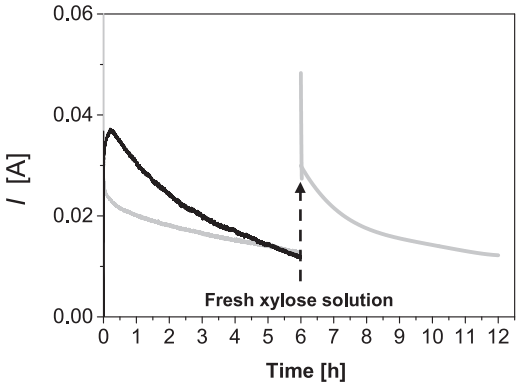

Fig. 10. *I*(t) curves recorded at 0.4 V and 293 K in the 25 cm^2 electrolysis cell for the oxidation of 0.1 M glucose (black line) and 0.1 M xylose (grey line) in 0.1 M NaOH aqueous solutions.

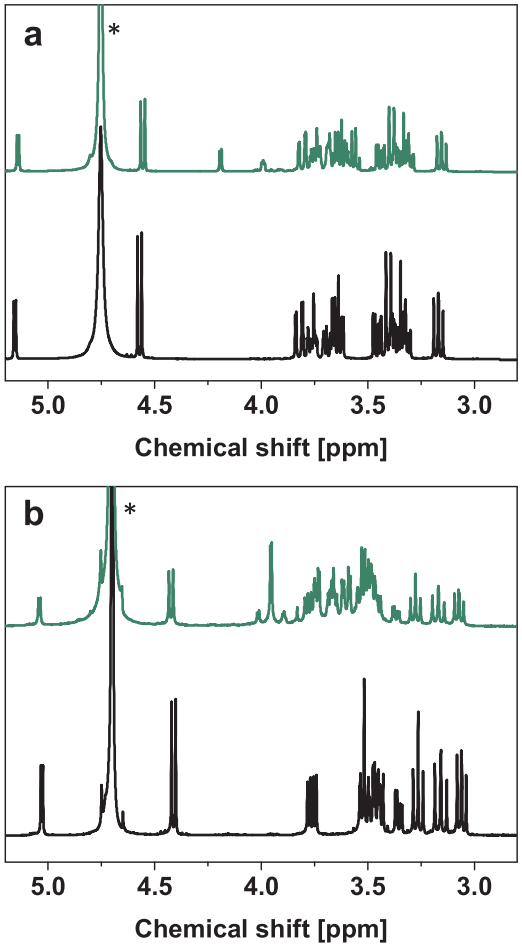

Fig. 11. ^{1}H NMR spectra of (a) glucose 0.1 M, NaOH 0.1 M and (b) xylose 0.1 M, NaOH 0.1 M solutions after neutralization with HCl, lyophilization and dissolution into D_2O. The spectra correspond to the initial solution before electrolysis (black curves) and after 6 h of electrolysis (green curves) normalized with respect to the internal reference (acetic acid, 0.03 M, δ = 2.1 ppm). The * correspond to HOD signal from the solvent (For interpretation of the references to colour in this figure legend, the reader is referred to the web version of this article).

voltage of 0.4 V for 6 h for both glucose and xylose electro-reforming. The initial current of glucose electrolysis is *ca.* 0.037 A, whereas that of xylose is *ca.* 0.026 A, confirming the higher reactivity of glucose than that of xylose as observed by cyclic voltammetry. For both aldoses, the current decreases monotonously over the 6 h electrolysis time range down to *ca.* 0.012 A. At a so low anode potential, it is unlikely that the catalyst undergoes restructuration. Poisoning of the surface could occur. However, as shown in Fig. 10, using the same system (anode, cathode and separator) with a fresh xylose solution leads to recover currents close to the initial ones with the same progression for the subsequent 6 h. It appears then that the decay in current is mainly due to the depletion of glucose or xylose in the solution owing to their consumption.

The analyses by ^{1}H NMR of the reaction products after CA of 0.1 M of glucose solution and 0.1 M xylose solution at 0.4 V were performed at the end of the electrolysis measurements to confirm the nature of the compounds formed at the anode (Fig. 11a and b, respectively). Fig. 11a shows the ^{1}H NMR spectra for the initial glucose solution before electrolysis (black curve) and after 6 h of electrolysis (green curve) normalized with respect to the internal reference (acetic acid, 0.03 M, δ = 2.1 ppm). The ^{1}H NMR spectrum of the initial solution shows typical signals for glucose in water with several peaks in the 3.3–3.8 ppm range, two doublets at δ = 4.6 ppm and δ = 5.2 ppm, typical of the hydrogen on the anomeric carbon of the α and β forms, respectively, and one doublet of doublets at δ = 3.2 ppm attributed to the hydrogen on the carbon next to the anomeric carbon of the β form of glucose. After 6 h of electrolysis, the signal of glucose has decreased and the global amount and position of peaks in the 3.3 to 3.8 ppm range has changed. Furthermore, a triplet and a doublet of peaks have appeared at δ = 4.0 ppm and δ = 4.2 ppm, respectively. They are typical of sodium gluconate (reference prepared from D-gluconic acid sodium salt, ≥99%, Sigma Aldrich). The Fig. 11b shows the ^{1}H NMR spectra for the initial xylose solution before electrolysis (black curve) and after 6 h of electrolysis (green curve) normalized with respect to the internal reference (acetic acid, 0.03 M, δ = 2.1 ppm). As observed for glucose, the ^{1}H NMR spectrum of the initial solution shows typical signals for xylose in water with several peaks in the 3.0 to 3.6 ppm range, two doublets at δ = 4.4 ppm and δ = 5.1 ppm, typical of the hydrogen on the anomeric carbon of the α and β forms, respectively, and a quadruplet of peaks at δ = 3.75 ppm attributed to the hydrogen on the carbon next to the anomeric carbon of the β form of xylose. After 6 h of electrolysis, again the signal of xylose has decreased and the global amount and position of peaks in the 3.0 to 3.8 ppm range has changed. One triplet and two doublets have appeared at δ = 3.8, δ = 3.9 and δ = 4.0, respectively. They are typical of presence of xylonate (reference prepared from D-xylonic acid lithium salt, ≥95.0%, Sigma Aldrich). Looking more closely to the ^{1}H NMR spectra (SI 3), some small peaks are attributed to the formation of small amount of xylonate and of trace of threonate in the case of glucose oxidation, and of threonate in the case of xylose oxidation (reference prepared from L-threonic acid hemicalcium salt, > 97%), Sigma aldrich).

To go further into the identification and quantification of reaction products, an aliquot of 0.6 mL of solution was sampled every hour using a microsyringe and analyzed by HPLC. Fig. 12a and b give the evolution of the chromatograms with the time of glucose and xylose electrolysis, respectively, together with the reference chromatograms of gluconic and xylonic acids. The black lines in both figures represent the chromatograms recorded on glucose and xylose 0.1 M solutions. Because these molecules don't bear chromophores, they are not detected using a UV detector set at a wavelength of 210 nm A refractometer as detector was also useless to determine the glucose and xylose concentrations because in our set-up they were detected at the same retention times as gluconic and xylonic acids, respectively. In both figures, the main peaks detected at *ca.* 7.6 min for glucose oxidation (Fig. 12a) and *ca.* 7.9 min for xylose oxidation (Fig. 12b) clearly correspond to gluconic and xylonic acids, respectively. In both cases a peak appears at a retention time of *ca.* 6.7 min. This peak couldn't be univocally attributed to a given species. This peak is already present after 1 h electrolysis and does not increase for longer times. It could correspond to the injection peak or it could come from the formation of other compounds in a very small amount at the very early stage of the electrolysis experiments as it does not increase. We propose that it could be due to the presence of an impurity in glucose and xylose commercial samples (such as fructose, which is an isomer of glucose), which is rapidly oxidized explaining the invariance of the peak intensity. As a matter of fact, this impurity is in a very small amount as it disappears after less than 1 h electrolysis. The main peaks of the chromatograms at 7.6 and 7.9 min for glucose and xylose oxidation reactions, respectively, were used to determine the gluconate and xylonate concentrations (and further $C_{glu,exp}$ and $C_{xyl,exp}$) by rescaling the gluconate (xylonate) reference chromatogram until it fits with the one recorded after a given electrolysis time. Then, by subtracting both chromatograms, we were able to identify additional small peaks which corresponded to other formed compounds (SI 4). In the case of glucose electrooxidation, two additional small peaks evidenced the presence of small xylonate amounts and traces of threonate, and a unique small peak evidenced the presence of small threonate amount in the case of xylose, confirming ^{1}H NMR results.

Fig. 13a and b compare $C_{glu,exp}$ and $C_{xyl,exp}$ with the theoretical number of moles determined from the Faraday's law, $C_{glu,theo}$ and

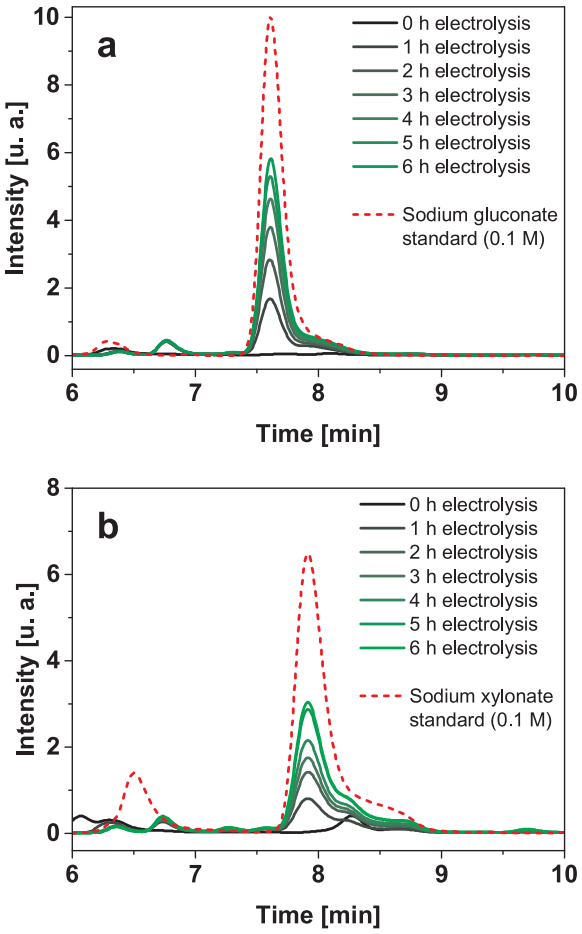

Fig. 12. Chromatograms recorded as a function of time during the electrolysis. (a) 0.1 M glucose and (b) 0.1 M xylose in 0.1 M NaOH aqueous solutions. The electrolysis time is presented with shades of green from 0 h (black) to 6 h (light green). The chromatograms for standard solutions at 0.1 M of (a) sodium gluconate and (b) lithium xylonate are shown (red dashed curve). (For interpretation of the references to colour in this figure legend, the reader is referred to the web version of this article).

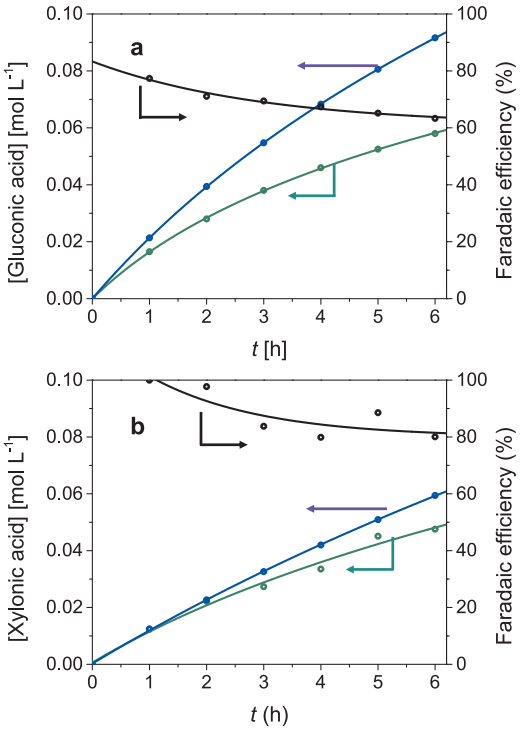

Fig. 13. (a) Comparison of the theoretical concentration of gluconate assuming a 100% selectivity (blue line) with the experimental one determined by HPLC (green line) and faradaic efficiency for gluconate production (black line) as a function of electrolysis time; (b) Comparison of the theoretical concentration of xylonate assuming a 100% selectivity (blue line) with the experimental one determined by HPLC (green line) and faradaic efficiency for the production of xylonate (black line) as a function of electrolysis time (For interpretation of the references to colour in this figure legend, the reader is referred to the web version of this article).

$C_{xyl,theo}$, which were expected assuming only the formation of gluconate and xylonate *via* a two-electron process. The resulting faradaic efficiency for the formation of gluconate or xylonate from both aldoses can be determined using the Eq. (13):

$$\eta_F = \frac{C_{glu(xyl),exp}}{C_{glu(xyl)theo}} \quad (13)$$

where $C_{glu(xyl),theo}$ and $C_{glu(xyl),exp}$ are the theoretical concentration of gluconate or xylonate determined from the Faraday law and the experimental concentrations determined from HPLC measurements, respectively.

The curves for both aldoses do not overlap, indicating that other products are formed, which were not directly detected by HPLC. The peak at *ca.* 6.7 min could correspond to one of these species. But, the fact that it does not increase with time cannot explain the increasing difference between the curves as a function of time. This also shows that the increase of reaction times leads to an increase of conversion rate, but due to the consumption of initial reactants, their concentrations at the electrode surface decrease and other oxidation reactions will take place at the electrode involving the first reaction products as intermediates. Therefore, the gain in conversion for longer reaction times will be at the expense of the selectivity (*i.e.*, the selectivity increases with decreasing the reaction time). Nevertheless, if other compounds are formed, they necessary correspond to highly oxidized ones. It can be reasonably proposed that these compounds come from further oxidations of gluconate into xylonate and xylonate into threonate (both with concomitant formation of CO_2), as both these compounds were detected by HPLC and ^{1}H NMR, according to the following electrochemical reactions:

$$\text{Glucose: } C_6H_{12}O_6 + 9\ OH^- \rightarrow C_5H_9O_6^- + CO_3^{2-} + 6\ H_2O + 6\ e^- \quad (14)$$

$$C_6H_{12}O_6 + 15\ OH^- \rightarrow C_4H_7O_5^- + 2\ CO_3^{2-} + 10\ H_2O + 10\ e^- \quad (15)$$

$$\text{Xylose: } C_5H_{10}O_5 + 9\ OH^- \rightarrow C_4H_7O_5^- + CO_3^{2-} + 6\ H_2O + 6\ e^- \quad (16)$$

Furthermore, in both scenarios, the number of exchanged electrons per molecule produced is higher than the number of electrons required for the production of one molecule of gluconate or xylonate (2 electrons), and even with a 65% and 80% faradaic efficiency after 6 h for glucose and xylose oxidation, respectively, the concentration of by-products may remain very low and the selectivities towards the formation of gluconate and xylonate remain high.

The concentration of glucose after 6 h electrolysis has been determined after reaction with a Fehling solution and analysis by UV–vis spectroscopy using a calibration curve (SI 1). A concentration of *ca.* 0.033 mol L^{-1} was determined (confirmed by HPLC on a Aminex column for carbohydrate separation), indicating that *ca.* 0.067 moL L^{-1} glucose were consumed (conversion rate of 67%). After 6 h electrolysis, *ca.* 0.058 moL L^{-1} of gluconate were obtained (Fig. 13a), so that *ca.* 0.009 mol L^{-1} of glucose have been consumed to form other compounds (selectivity towards gluconate of 87%). The formation of xylonate and threonate, the only by-products determined by HPLC and ^{1}H

NMR, with simultaneous production of CO_2, involves the consumption of 6 and 10 electrons, respectively, instead of 2 for the formation of gluconate (*i.e.* 3 and 5 times more, respectively). If assuming the only formation of gluconate with 2 mol of electrons involved per mole of glucose oxidized, 0.0916 mol L^{-1} of gluconate should be obtained instead of 0.058 mol L^{-1} (Fig. 13a). Now the production of xylonate (x mol L^{-1}) and threonate (t mol L^{-1}) can be determined by resolving the following system of equations:

$$x + t = 0.009 \text{ mol } L^{-1} \quad (17)$$

$$3x + 5t + 0.058 = 0.0916 \text{ mol } L^{-1} \quad (18)$$

which leads to x = 0.0057 mol L^{-1} of xylonate (ten times less than gluconate) and y = 0.0033 mol L^{-1} of threonate imes less than gluconate)

The same reasoning has been applied to xylose electro-oxidation. In this case, 0.048 mol L^{-1} of xylose remained after 6 h electrolysis. Therefore 0.052 mol L^{-1} were consumed to produce 0.0476 mol L^{-1} of xylonate (Fig. 13b) and 0.0044 mol L^{-1} were transformed into other compounds (conversion rate of 52% and selectivity towards xylonate of 92%). Because only threonate has been detected as byproduct, then:

$$3t + 0.0476 = 3 \times (0.0044) + 0.04756 = 0.0608 \text{ mol } L^{-1} \quad (19)$$

This value is very close to that for the theoretical concentration $C_{xyl,theo(}6\,h) = 0.0594$ mol L^{-1} (Fig. 13b). This indicates that in case of xylose electrooxidation, no other product is formed.

The only formation of xylonate (with CO_2) involving 6 electrons per molecule oxidized (Eq. (14)), *i.e.* 3 times more than for gluconate, and the only formation of threonate (with CO_2) involving 10 electrons per molecule oxidized (Eq. (15)), *i.e* 5 times more than for gluconate, represent the limit scenarios of glucose oxidation. In the case of xylose, only threonate was detected as byproduct, the formation of which involves 6 electrons (Eq. (16)), *i.e* 3 times more than for xylonate. From these limit scenarios, it is possible to calculate at different reaction times the concentration limits of aldoses ($C^{6e-}_{Glucose}(t)$, $C^{10e-}_{Glucose}(t)$ and $C^{6e-}_{Xylose}(t)$), the conversion limits of aldoses ($X^{6e-}_{Glucose}(t)$, $X^{10e-}_{Glucose}(t)$ and $X^{6e-}_{Xylose}(t)$), and further the selectivity limits in gluconate and xylonate ($S^{6e-}_{Gluconate}(t)$, $S^{10e-}_{Gluconate}(t)$ and $S^{6e-}_{Xylonate}(t)$), according to the following equations:

$$C_i^{6e-}(t) = 0.1 - C_{j,exp}(t) - \frac{C_{j,theo}(t) - C_{j,exp}(t)}{3} \quad (20)$$

$$C_i^{10e-}(t) = 0.1 - C_{j,exp}(t) - \frac{C_{j,theo}(t) - C_{j,exp}(t)}{5} \quad (21)$$

$$X_i^{6e-}(t) = \frac{0.1 - C_i^{6e-}(t)}{0.1} \quad (22)$$

$$X_i^{10e-}(t) = \frac{0.1 - C_i^{10e-}(t)}{0.1} \quad (23)$$

$$S_j^{6e-}(t) = \frac{C_{j,exp}(t)}{0.1 - C_i^{6e-}(t)} \quad (24)$$

$$S_j^{10e-}(t) = \frac{C_{j,exp}(t)}{0.1 - C_i^{10e-}(t)} \quad (25)$$

where *t* is the reaction time in hour, the index i refers to glucose or xylose and the index j refers to gluconate or xylonate.

Results are given in Table 2. For 6 h electrolysis of glucose, the conversion rates and the selectivity values obtained from HPLC measurements are within the intervals of the calculated limit scenario values obtained. In the case of xylose, after 6 h electrolysis the same values of 52% and 92% for conversion rate and selectivity, respectively, are obtained by calculations and from HPLC measurements. Both these results confirm the accuracy of the method for determining the reaction selectivity with respect to the reaction time.

In the case of glucose, the selectivity in gluconate is comprised between 91% and 98% for *ca.* 18% conversion (1-h electrolysis). The selectivity falls down to 87% after 6 h electrolysis with a glucose conversion of 67% but remains still high. In the case of xylose, the results are still better, with a selectivity towards xylonate of 100% after 2 h electrolysis (22% conversion), which reaches 92% after 6 h electrolysis (52% conversion).

The very high selectivities in gluconate and moreover in xylonate at very low cell voltage imply that the production of these value-added products can be performed with low electrical energy consumption. The counter reaction in the electrolysis cell being the hydrogen evolution reaction (Eq. (10)), the electrical energy to produce 1 kg of hydrogen at 0.4 V is 10.73 kW h kg_{H2}^{-1}. The theoretical energy needed to produce 1 kg of hydrogen from water under standard conditions at the standard equilibrium voltage of 1.23 V is 33 kW h kg^{-1} [38], hence the saccharide electrolysis can also provide high purity hydrogen for one third of the theoretical energy required from water electrolysis. If the faradaic yield in gluconic/xylonic acid was 100%, then the energy of 10.73 kW h would lead to the production of 98 kg of gluconic acid or 83 kg of xylonic acid (500 mol for both), *i.e.* 0.02144 kW h mol_{Aldose}^{-1} or 77.188 kJ mol_{Aldose}^{-1}. Considering the lowest faradaic yields of 63.3% for gluconic acid and of 80.1% for xylonic acid in Table 2, the electrical energy consumed of 10.73 kW h allows the simultaneous production of 1 kg of hydrogen at the cathode and of *ca.* 62 kg of gluconic acid (316.3 mol, 0.03392 kW h $mol_{Glucose}^{-1}$, 122.11 kJ $mol_{Glucose}^{-1}$) or *ca.* 67.3 kg of xylonic acid (405.2 mol, 0.02648 kW h mol_{Xylose}^{-1}, 95.33 kJ mol_{Xylose}^{-1}) at the anode. Now, considering the mean electricity cost in Europe (*ca.* 0.20 € / kWh) [68], the energy cost for the production of 1 ton of gluconic or xylonic acid will range between 32 € and 36 € / ton (with co-production of 12 to 13 kg of high purity hydrogen). This cost represent less than 7% of the global cost of gluconic acid or sodium gluconate industrially produced using biotechnological processes, which ranges between *ca.* 600 to *ca.* 750 US $ (520 to 650 €) per ton (Dezhou Huiyang Biotechnology Co., Ltd, Wuxi Fengmin Environmental Technology Development Co., Ltd, *etc.*).

4. Conclusion

Nanocatalysts based on palladium and gold have been synthesized by a water-in-oil microemulsion route. Pd_xAu_{10-x}/C nanosized materials with different atomic compositions have been characterized. Their activity and selectivity toward glucose and xylose electrooxidation has been investigated by cyclic voltammetry and *in situ* FTIRS measurements. The best catalyst composition, in terms of lower oxidation onset potential, higher activity and better selectivity towards gluconate and xylonate, was Pd_3Au_7/C. At last, chronoamperometry measurements in a 25 cm^2 elecrolysis cell were conducted at the low potential of 0.4 V and at the low temperature of 293 K for 6 h and the reaction products were analyzed. Several new insights were pointed out:

- Pd and Au are alloyed in the bimetallic structures;
- The surface composition of Pd_xAu_{10-x} is different than the bulk one, being enriched in palladium with respect to the bulk composition determined by AAS;
- The adsorption of aldoses at low potentials on Pd rich catalysts is dissociative leading to CO_{ads} species, whereas for catalysts with Au content ≥70 at%, this reaction is avoided;
- Much lower onset potentials (*ca.* 0.1 V vs RHE), higher tolerance to poisoning and higher selectivity towards gluconate or xylonate were obtained with Pd_3Au_7/C catalyst for glucose and xylose oxidation, than those proposed for Pt- [29], Pd- [69] and Au-based [32,34], electrocatalytic surfaces in the literature under similar experimental conditions;
- Selectivity towards gluconate was 87% for a glucose conversions of 67%, and higher for lower electrolysis times (lower conversion);
- Selectivity towards xylonate was higher than 92% for a conversion

Table 2
Electrolysis and HPLC data for the calculation of the aldose conversion and selectivities in gluconate and xylonate.

Glucose

Time (h)	Q_{Elec} (C)	$C_{glu,theor}$ (mol L^{-1})	$C_{glu.,exp.}$ (mol L^{-1})	η_F (%)	$C^{6e^-}_{Glucose}$ (mol L^{-1})	$C^{10e^-}_{Glucose}$ (mol L^{-1})	$X^{6e-}_{Glucose}(t)$ (%)	$X^{10e-}_{Glucose}(t)$ (%)	$S^{6e-}_{Gluconic}(t)$ (%)	$S^{10e-}_{Gluconic}(t)$ (%)
1	121	0.0165	0.0213	77.4	0.0820	0.0825	18.1	17.5	91.1	94.5
2	219	0.0280	0.0394	71.1	0.0682	0.0697	31.8	30.2	88.1	92.5
3	298	0.0380	0.0547	69.4	0.0564	0.0587	43.6	41.4	87.2	91.9
4	364	0.0460	0.0683	67.4	0.0466	0.0495	53.4	50.5	86.1	90.3
5	420	0.0525	0.0801	65.2	0.0381	0.0419	61.9	58.1	84.9	95.7
6	466	0.0580	0.0916	63.3	0.0308	0.0353	69.2	64.7	83.8	89.6

Xylose

Time (h)	$Q_{Elec.}$ (C)	$C_{Xyl.,theor.}$ (mol L^{-1})	$C_{Xyl.,exp.}$ (mol L^{-1})	η_F (%)	$C^{6e^-}_{Xylose}$ (mol L^{-1})	$X^{6e-}_{Xylose}(t)$ (%)	$S^{L,6}_{Xylonic}(t)$ (%)
1	68	0.0124	0.0124	100	0.0876	12.4	100
2	126	0.0222	0.0227	97.7	0.0777	22.3	99.2
3	177	0.0273	0.0326	83.8	0.0709	29.1	93.9
4	224	0.0335	0.0420	79.9	0.0637	36.3	92.2
5	265	0.0451	0.0509	88.5	0.0530	47.0	95.9
6	303	0.0477	0.0594	80.1	0.0485	51.5	92.3

of 45%, reaching 100% for 1 and 2 h electrolysis;
- Such high selectivities at so low cell voltages imply that the electric energy cost needed for to produce 1 ton of gluconic acid and xylonic acid (associated with the co-production of 12–13 kg of high purity hydrogen) is lower than 36 €, which is industrially very interesting for decreasing the operating expenditures. Indeed, the cost of gluconic acid or sodium gluconate industrially produced using biotechnological processes ranges between *ca.* 600–750 US $ (520–650 €) per ton (Dezhou Huiyang Biotechnology Co., Ltd, Wuxi Fengmin Environmental Technology Development Co., Ltd, *etc.*).

The present study proposes a catalyst which, conversely to other Pt- and Pd- based catalysts usually used, allowed the oxidation of glucose/xylose at very low potentials (onset potentials lower than 0.1 V vs RHE), without C—C bond breaking (no CO observed by *in-situ* infrared spectroscopy). In the literature, only one paper could be found regarding the glucose electrooxidation on PdAu bimetallic catalysts. Much higher poisoning tolerance during glucose oxidation was obtained with the alloyed Pd_3Au_7/C catalyst developed in the present work than with the non-alloyed Pd_3Au_7/C catalyst described in the literature. Indeed, an important shift of the onset potential towards lower values was obtained with our alloyed catalysts (compared to pure Pd and Au catalysts) leading to much lower values of onset potential than those obtained with non-alloyed PdAu catalysts from the literature.

This work corresponds to a proof of concept, which explains the reason why we have used low concentrations of glucose and xylose, and low metal loadings in the electrodes (generally, anodes for organics electrooxidation are loaded with several mg of metal per cm^2) [70]. Obviously, it opens the door to deeper studies and improvements of the system. For example, if the energy consumption is low, the rate of production must be increased. The metal loading in the anodes could be increased, as well as the concentrations of aldoses and NaOH in the solutions (as it is the case for glycerol electrooxidation) [24]. Other catalysts can also be developed to shift the oxidation onset potential towards lower values and to enhance the turn over frequency at low potential (to decrease the surface poisoning). The investigations on all these aspects are currently under progress in our laboratory.

Acknowledgements

The authors thank the European communities (FEDER), the “Région Nouvelle Aquitaine” and the PHC Tournesol (French-Belgian cooperation Hubert Curie) for financial supports.

Appendix A. Supplementary data

Supplementary material related to this article can be found, in the online version, at doi:https://doi.org/10.1016/j.apcatb.2018.11.006.

References

[1] T. Werpy, G. Petersen, A. Aden, J. Bozell, J. Holladay, J. White, A. Manheim, D. Elliot, L. Lasure, S. Jones, M. Gerber, K. Ibsen, L. Lumberg, S. Kelley, Pacific Northwest National Laboratory, National Renewable Energy Laboratory. Top Value Added Chemicals from Biomass: Results of Screening for Potential Candidates from Sugars and Synthesis Gas, Department of Energy, Oak Ridge, TN, 2004.
[2] H. Liu, K.N.G. Valdehuesa, G.M. Nisola, K.R.M. Ramos, W.-J. Chung, High yield production of D-xylonic acid from D-xylose using engineered Escherichia coli, biores, Technol. 115 (2012) 244–248.
[3] A.M. Cañete-Rodríguez, I.M. Santos-Dueñas, J.E. Jiménez-Hornero, A. Ehrenreich, W. Liebl, I. García-García, Gluconic acid: properties, production methods and applications - an excellent opportunity for agro-industrial by-products and waste biovalorization, Proc. Biochem. 51 (2016) 1891–1903.
[4] H. Hustede, H.-J. Haberstroh, E. Schinzig, Gluconic acid, Ullmann’s Encyclopedia of Industrial Chemistry, 7th ed., Wiley on line library, 2007.
[5] M.J. Climent, A. Corma, S. Iborra, Converting carbohydrates to bulk chemicals and fine chemicals over heterogeneous catalysts, Green Chem. 13 (2011) 520–540.
[6] A. Tathod, T. Kane, E.S. Sanil, P.L. Dhepe, Solid base supported metal catalysts for the oxidation and hydrogenation of sugars, J. Mol. Catal. A: Chem. 388–389 (2014) 90–99.
[7] A. Onda, T. Ochi, K. Kajiyoshi, K. Yanagisawa, A new chemical process for catalytic conversion of D-glucose into lactic acid and gluconic acid, Appl. Catal. A Gen. 343 (2008) 49–54.
[8] A. Mirescu, U. Prüße, A new environmental friendly method for the preparation of sugar acids via catalytic oxidation on gold catalysts, Appl. Catal. B: Environ. 70 (2007) 644–652.
[9] X. Liang, C.-J. Liu, P. Kuai, Selective oxidation of glucose to gluconic acid over argon plasma reduced Pd/Al_2O_3, Green Chem. 10 (2008) 1318–1322.
[10] P. Gallezot, Selective oxidation with air on metal catalysts, Catal. Today 37 (1997) 405–418.
[11] S. Karski, I. Witónska, Bismuth as an additive modifying the selectivity of palladium catalysts, J. Mol. Catal. A: Chem. 191 (2003) 87–92.
[12] S. Karski, Activity and selectivity of $Pd–Bi/SiO_2$ catalysts in the light of mutual interaction between Pd and Bi, J. Mol. Catal. A: Chem. 253 (2006) 147–154.
[13] S. Biella, L. Prati, M. Rossi, Selective oxidation of D-glucose on gold catalyst, J. Catal. 206 (2002) 242–247.
[14] M. Comotti, C. Della Pina, R. Matarrese, M. Rossi, The catalytic activity of “naked” gold particles, Angew. Chem. Int. Ed. 43 (2004) 5812–5815.
[15] C. Baatz, U. Prüße, Preparation of gold catalysts for glucose oxidation by incipient wetness, J. Catal. 249 (2007) 34–40.
[16] C. Della Pina, E. Falletta, Gold-catalyzed oxidation in organic synthesis: a promise kept, Catal. Sci. Technol. 1 (2011) 1564–1571.
[17] P. Bujak, P. Bartczak, J. Polanski, Highly efficient room-temperature oxidation of cyclohexene and D-glucose over nanogold Au/SiO_2 in water, J. Catal. 295 (2012)

15–21.
[18] D. Rinsant, G. Chatel, F. Jérôme, Efficient and selective oxidation of d-glucose into gluconic acid under low-frequency ultrasonic irradiation, ChemCatChem 6 (2014) 3355–3359.
[19] M. Omri, G. Pourceau, M. Becuwe, A. Wadouachi, Improvement of gold-Catalyzed oxidation of free carbohydrates to corresponding aldonates using microwaves, ACS Sustain. Chem. Eng. 4 (2016) 2432–2438.
[20] M. Simões, S. Baranton, C. Coutanceau, Electrochemical valorization of glycerol, ChemSusChem 5 (2012) 2106–2124.
[21] A. Zalineeva, M. Padilla, U. Martinez, A. Serov, K. Artyushkova, S. Baranton, C. Coutanceau, P.B. Atanassov, Self-supported Pd-Bi catalysts for the electro-oxidation of glycerol in alkaline media, J. Am. Chem. Soc. 136 (2014) 3937–3945.
[22] C. Coutanceau, A. Zalineeva, S. Baranton, M. Simões, Modification of palladium surfaces by bismuth adatoms or clusters: effect on electrochemical activity and selectivity towards polyol electrooxidation, Int. J. Hyd. Energy 39 (2014) 15877–15886.
[23] J. Cobos-Gonzalez, S. Baranton, C. Coutanceau, A systematic in situ infrared study of the electrooxidation of C3 alcohols on Pt_9Bi_1/C catalysts, J. Phys. Chem. C 120 (2016) 7155–7164.
[24] J. Cobos-Gonzalez, S. Baranton, C. Coutanceau, Development of Bi-modified PtPd nanocatalysts for the electrochemical reforming of polyols into hydrogen and value-added chemicals, ChemElectroChem 3 (2016) 1694–1704.
[25] A. Brouzgou, P. Tsiakaras, Electrocatalysts for glucose electrooxidation reaction: a review, Top. Catal. 58 (2015) 1311–1327.
[26] M. Pasta, F. La Mantia, Y. Cui, Mechanism of glucose electrochemical oxidation on gold surface, Electrochim. Acta 55 (2010) 5561–5568.
[27] A. Heller, B. Feldman, Electrochemical glucose sensors and their applications in diabetes management, Chem. Rev. 108 (2008) 2482–2505.
[28] K.E. Toghill, R.G. Compton, Electrochemical non-enzymatic glucose sensors: a perspective and an evaluation, Int. J. Electrochem. Sci. 5 (2010) 1246–1301.
[29] A.T. Governo, L. Proença, P. Parpot, M.I.S. Lopes, I.T.E. Fonseca, Electro-oxidation of D-xylose on platinum and gold electrodes in alkaline medium, Electrochim. Acta 49 (2004) 1535–1545.
[30] A. Cardoso de Sá, L. Lataro Paim, N. Ramos Stradiotto, Sugars electrooxidation at glassy carbon electrode decorate with multi-walled carbon nanotubes with nickel oxy-hydroxide, Int. J. Electrochem. Sci. 9 (2014) 7746–7762.
[31] B. Beden, F. Largeaud, K.B. Kokoh, C. Lamy, Fourier transform infrared reflectance spectroscopic investigation of the electrocatalytic oxidation of D-glucose: identification of reactive intermediates and reaction products, Electrochim. Acta 41 (1996) 701–709.
[32] M. Tominaga, M. Nagashima, K. Nishiyama, I. Taniguchi, Surface poisoning during electrocatalytic monosaccharide oxidation reactions at gold electrodes in alkaline medium, Electrochem. Commun. 9 (2007) 1892–1898.
[33] S. Hermans, A. Deffernez, M. Devillers, Au–Pd/C catalysts for glyoxal and glucose selective oxidations, Appl. Catal. A: Gen. 395 (2011) 19–27.
[34] L. Yan, A. Brouzgou, Y. Meng, M. Xiao, P. Tsiakaras, S. Song, Efficient and poison-tolerant Pd_xAu_y/C binary electrocatalysts for glucose electrooxidation in alkaline medium, Appl. Catal. B: Environ. 150–151 (2014) 268–274.
[35] M. Mougenot, A. Caillard, M. Simões, S. Baranton, C. Coutanceau, P. Brault, PdAu/C catalysts prepared by plasma sputtering for the electro-oxidation of glycerol, Appl. Catal. B: Environ. 107 (2011) 372–379.
[36] F. Largeaud, K.B. Kokoh, B. Beden, C. Lamy, On the electrochemical reactivity of anomers: electrocatalytic oxidation of LX– and P-D-glucose on platinum electrodes in acid and basic media, J. Electroanal. Chem. 397 (1995) 261–269.
[37] M. Simões, S. Baranton, C. Coutanceau, Electrooxidation of sodium borohydride ($NaBH_4$) at Pd, Au and Pd_xAu_{1-x} carbon supported nanocatalysts, J. Phys. Chem. C 113 (2009) 13369–13376.
[38] C. Lamy, A. Devadas, M. Simões, C. Coutanceau, Clean hydrogen production through the electrocatalytic oxidation of formic acid in a PEM electrolysis cell (PEMEC), Electrochim. Acta 60 (2012) 112–120.
[39] S. Lankiang, M. Chiwata, S. Baranton, H. Uchida, C. Coutanceau, Oxygen reduction reaction at binary and ternary nanocatalysts based on Pt, Pd and Au, Electrochim. Acta 182 (2015) 131–142.
[40] W.S. Rasband, Image J, US National Institutes of Health, Bethesda, MD, USA, 2009http://rsbweb.nih.gov/ij/.
[41] B. Beden, C. Lam, R.J. Gale (Ed.), Spectroelectrochemistry: Theory and Practice, Plenum Press, New York, 1988Chapter 5, pp 189 – 261.
[42] A. Kabbabi, R. Faure, R. Durand, B. Beden, F. Hahn, J.-M. Léger, C. Lamy, In situ FTIRS study of the electrocatalytic oxidation of carbon monoxide and methanol at Platinum – Ruthenium bulk alloy electrodes, J. Electroanal. Chem. 444 (1998) 41–53.
[43] M. Wojdyr, Fityk: a general-purpose peak fitting program, J. Appl. Crystal. 43 (2010) 1126–1128.
[44] B.E. Warren, X-Ray Diffraction, Dover Publications, Inc., New York, 1990.
[45] M. Grdén, M. Lukaszewski, G. Jerkiewicz, A. Czerwinski, Electrochemical behaviour of palladium electrode: oxidation, electrodissolution and ionic adsorption, Electrochim. Acta 53 (2008) 7583–7598.
[46] A.N. Kahyaoglu, Oxydation Electrocatalytique du Glycérol sur le Platine, l'Or et leurs Alliages Binaires. Ph.D. Thesis, University of Poitiers, Poitiers, France, 1981 p. 80.
[47] A.J. Rand, R. Woods, Determination of surface composition of smooth noble metal alloys by cyclic voltammetry, J. Electroanal. Chem. 57 (1972) 57–69.
[48] P.J. Cumpson, M.P. Seah, Elastic scattering corrections in AES and XPS. II. Estimating attenuation lengths and conditions required for their valid use in overlayer/substrate experiments, Surf. Interface Anal. 25 (1997) 430–446.
[49] A. Jablonski, H. Ebel, Comparison of electron attenuation lengths and escape depths with inelastic mean free paths, Surf. Interface Anal. 11 (1988) 627–632.
[50] A. Jablonski, H. Ebel, Effects of elastic photoelectron collisions in quantitative XPS, Surf. Interface Anal. 6 (1984) 21–28.
[51] M. Łukaszewski, A. Czerwiński, Electrochemical preparation and characterization of thin deposits of Pd-noble metal alloys, Thin Solid Films 518 (2010) 3680–3689.
[52] M.L. Avramov-Ivić, J.M. Léger, C. Lamy, V.D. Jović, S.D. Petrović, The electro-oxidation of glycerol on the gold (100)-oriented single-crystal surface and poly crystalline surface in 0.1 m NaOH, J. Electroanal. Chem. 308 (1991) 309–317.
[53] H.–W. Lei, B. Wu, C.–S. Cha, H. Kita, Electro-oxidation of glucose on platinum in alkaline solution and selective oxidation in the presence of additives, J. Electroanal. Chem. 382 (1995) 103–110.
[54] S. Ernst, J. Heitbaum, C.H. Hamann, The electrooxidation of glucose in phosphate buffer solutions: part I. Reactivity and kinetics below 350 mV/RHE, J. Electroanal. Chem. Interfacial Electrochem. 100 (1979) 173–183.
[55] B. Beden, I. Cetin, A. Kahyaoglu, D. Takky, C. Lamy, Electrocatalytic oxidation of saturated oxygenated compounds on gold electrodes, J. Catal. 104 (1987) 37–46.
[56] R.R. Adzic, M.W. Hsiao, E.B. Yeager, Electrochemical oxidation of glucose on single crystal gold surfaces, J. Electroanal. Chem. Interfacial Electrochem. 260 (1989) 475–485.
[57] M. Watanabe, S. Motoo, Electrocatalysis by ad-atoms: part II. Enhancement of the oxidation of methanol on platinum by ruthenium ad-atoms, J. Electroanal. Chem. 60 (1975) 267–273.
[58] Y.Y. Tong, H.S. Kim, P.K. Babu, P. Waszczuk, A. Wieckowski, E. Oldfield, An NMR investigation of CO tolerance in a Pt/Ru fuel cell catalyst, J. Am. Chem. Soc. 124 (2002) 468–473.
[59] T. Iwasita, F.C. Nart, W. Vielstich, An FTIR study of the catalytic activity of a 85:15 Pt:Ru alloy for methanol oxidation, Ber. Bunsenges. Phys. Chem. 94 (1990) 1030–1034.
[60] T. Frelink, W. Visscher, J.A.R. van Veen, Measurement of the Ru surface content of electrocodeposited PtRu electrodes with the electrochemical quartz crystal microbalance: implications for methanol and CO electrooxidation, Langmuir 12 (1996) 3702–3708.
[61] C.J. Pouchert, The Aldrich Library of Infrared Spectra, 3rd ed., Aldrich Chemical Company, Inc., Milwaukee, WI, USA, 1981.
[62] Spectral Database for Organic Compounds (SDBS), National Institute of Advanced Industrial Science and Technology (AIST - Japan); http://sdbs.db.aist.go.jp/sdbs/cgi-bin/cre_index.cgi. (Accessed 20 July 2018).
[63] Y.-X. Jiang, S.-G. Sun, N. Ding, Novel phenomenon of enhancement of IR absorption of CO adsorbed on nanoparticles of Pd confined in supercages of Y-zeolite, Chem. Phys. Lett. 344 (2001) 463–470.
[64] A. Dailey, J. Shin, C. Korzeniewski, Ethylene glycol electrochemical oxidation at platinum probed by ion chromatography and infrared spectroscopy, Electrochim. Acta 44 (1998) 1147–1152.
[65] L. Dubau, F. Hahn, C. Coutanceau, J.-M. Léger, C. Lamy, On the structure effects of bimetallic PtRu electrocatalysts towards methanol oxidation, J. Electroanal. Chem. 554–555 (2003) 407–415.
[66] P.A. Christensen, A. Hamnett, The oxidation of ethylene glycol at a platinum electrode in acid and base, J. Electroanal. Chem. 260 (1989) 347–359.
[67] M. Simões, S. Baranton, C. Coutanceau, Enhancement of catalytic properties for glycerol electrooxidation on Pt and Pd nanoparticles induced by Bi surface modification, Appl. Catal. B: Environ. 110 (2011) 40–49.
[68] http://ec.europa.eu/eurostat/statistics-explained/index.php?title=Electricity_price_statistics/fr. (Accessed 23 August 2018).
[69] S. Song, K. Wang, L. Yan, A. Brouzgou, Y. Zhang, Y. Wang, P. Tsiakaras, Ceria promoted Pd/C catalysts for glucose electrooxidation in alkaline media, Appl. Catal. B: Environ. 176–177 (2015) 233–239.
[70] C. Coutanceau, S. Baranton, Electrochemical conversion of alcohols for hydrogen poduction: a short overview, WIREs Energy Environ. (2016) 388–400, https://doi.org/10.1002/wene.193.